

# Diffusion of divalent cations in garnet: multi-couple experiments

A. L. Perchuk · M. Burchard · H.-P. Schertl ·  
W. V. Maresch · T. V. Gerya · H.-J. Bernhardt ·  
O. Vidal

Received: 3 April 2008 / Accepted: 13 October 2008 / Published online: 23 November 2008  
© Springer-Verlag 2008

**Abstract** We demonstrate the possibility of studying several diffusion couples in a single run, i.e. under almost similar  $P$ – $T$ – $t$ – $f_{O_2}$  conditions, allowing direct comparison of the diffusion rates in different diffusion couples. Thus the duration of experimental study and the risk of failure of expensive experimental equipment can be decreased considerably. The diffusion experiments were carried out in piston-cylinder apparatus. Gem-quality garnets of almandine, spessartine and grossular compositions together with inclusion-rich eclogitic garnets were embedded in a powder of natural pyrope and annealed together under dry conditions at  $P = 1.9$ – $3.2$  GPa and  $T = 1,070$ – $1,400^\circ\text{C}$ . Diffusion profiles were measured by electron microprobe

and fitted numerically on the basis of multicomponent diffusion theory. The datasets derived from different diffusion couples yields parameters of the Arrhenius equation for Ca, Mg and Fe in natural eclogitic garnets and Mg, Mn and Fe in gem-quality garnets. We have also studied the effect of grain-boundary diffusion in the sintered pyrope matrix on interdiffusion on the basis of 2D modeling. Under conditions analogous to those of our experimental runs, we show that observed irregularities in some measured diffusion profiles (not applied for the diffusion modeling) can be directly related to the superposition of local grain-boundary diffusion on dominant volume diffusion.

---

Communicated by T.L. Grove.

---

A. L. Perchuk (✉)  
IGEM, Russian Academy of Sciences, Staromonetny 35,  
119017 Moscow, Russia  
e-mail: alp@igem.ru

A. L. Perchuk  
IEM, Russian Academy of Sciences,  
Chernogolovka 142432, Russia

M. Burchard  
Mineralogical Institute, University Heidelberg,  
69120 Heidelberg, Germany

H.-P. Schertl · W. V. Maresch · H.-J. Bernhardt  
Institute of Mineralogy, Geology and Geophysics,  
Ruhr-University Bochum, 44780 Bochum, Germany

T. V. Gerya  
ETH Zürich, Zurich, Switzerland

O. Vidal  
Laboratoire de Géodynamique des Chaînes Alpines,  
C.N.R.S, UMR 5025, Grenoble, France

**Keywords** Diffusion · Diffusion coefficient · Garnet ·  
Experiment · Piston-cylinder · Mineral inclusion ·  
Grain-boundary diffusion

## Introduction

Garnet is an important rock-forming mineral of various magmatic, metamorphic and metasomatic rocks. Because of the flexibility provided by many possible end-member compositions, garnets are formed in many different lithologies and at various  $P$ – $T$  conditions of the Earth's crust and mantle. The composition of garnet is very sensitive to these parameters and thus variations often lead to the formation of zoned crystals. A variety of zoning patterns in metamorphic garnets have been summarized in a number of publications (e.g. Tracy 1982; Chakraborty and Ganguly 1991; Perchuk and Philippot 2000). Garnet zoning is of particular interest, because it can be used to reconstruct rates of temperature and/or pressure variation of rocks from different geodynamic settings (e.g. Lasaga

1983; Muncill and Chamberlain 1988; Ganguly et al. 1996, 2000; Jiang and Lasaga 1990; Medaris et al. 1990; O'Brien and Vrana 1995; Gerasimov and Savko 1995; Carlson and Schwarze 1997; Perchuk et al. 1999; Dachs and Proyer 2002; Olker et al. 2003; Trepmann et al. 2004; Faryad and Chakraborty 2005). The procedure of deciphering the timescales of geologic processes on the basis of modeling diffusional modification of mineral composition(s) is known as geospeedometry (Lasaga 1983). Precise knowledge of the diffusion coefficients of diffusing species is crucial for this method. In the case of garnet, the diffusion rates of the four major divalent cations Ca, Fe, Mg and Mn are of primary interest.

Experimental studies of cation diffusion in garnets are usually carried out with gem-quality crystals close to end-member compositions. However, such crystals are rather rare in nature. Natural garnets are often chemically heterogeneous, often contain mineral inclusions and represent complex solid solution. In this contribution, we test a method of retrieving the diffusivity of Fe, Mn, Mg and Ca in different diffusion couples annealed together under almost identical  $P$ – $T$ – $t$ – $f_{O_2}$  conditions and compare the diffusivity of the major divalent cations in gem quality and inclusion-rich garnets. This study thus also provides additional data on the compositional effects of cation diffusion in garnet.

### Brief overview of previous experimental studies

A literature survey (Table 1) reveals that four principal experimental methods have been used to study diffusivities in garnet: (1) garnet crystals are embedded in a sintered powder of garnet of dissimilar composition (“CIP method”); (2) two garnet crystals of dissimilar composition are juxtaposed to form a “sandwich” (“SC method”); (3) a film containing a tracer isotope is coated over the surface of the garnet (“TC method”); (4) a self-developing overgrowth is induced on garnet seeds (“SOI method”).

The first experimental study of diffusivity in garnet was based on the CIP method with natural almandine crystals embedded in a powder of spessartine (Freer 1979). However, Elphick et al. (1985) later applied this method and could not find any measurable diffusion profile of Mg within the sintered almandine crystals. The lack of visible diffusion was interpreted as “preferential channeling of diffusion along tortuous grain boundaries”. This was in marked contrast to the useful diffusion profile in a similar annealing run using the SC method with sandwiched crystals of almandine and pyrope (Elphick et al. 1985). Later, Freer (1987) assessed his former data as “demonstrative” and the CIP method has not been used again in studies of diffusivities in garnet (see also Ganguly et al. 1987, for discussion).

The principal source of presently available diffusion data is based either on SC runs with sandwiched crystals (Elphick et al. 1985; Chakraborty and Ganguly 1992; Ganguly et al. 1998; Freer and Edwards 1999) or on TC experiments (Cygan and Lasaga 1985; Schwandt et al. 1995, 1996; Chakraborty and Rubie 1996). The SC method usually requires long run times and relatively high annealing temperatures ( $>1,000^\circ\text{C}$ ) to reach a diffusion penetration ( $>8\ \mu\text{m}$ ) sufficient for electron microprobe measurements (assuming a spatial resolution of  $\sim 4\ \mu\text{m}$ ). One of the uncertainties of this method arises from the necessary extrapolation of these data down to metamorphic temperatures below  $<1,000^\circ\text{C}$ . Such relatively low temperatures can be studied experimentally using the tracer isotope coating method. Such runs are commonly conducted at atmospheric pressure. There is, however, a single run at very high pressure by Chakraborty and Rubie (1996). Very narrow ( $<10^{-2}\ \mu\text{m}$ ) diffusion profiles of a trace isotope developed during diffusion anneals are measured by SIMS depth profiling.

SOI is a new experimental approach for studying diffusivity in garnet (Vielzeuf et al. 2005a, b, 2007). It is closely mimics natural occurrences in which interdiffusion occurs between an original garnet core and overgrowths of different composition (e.g. Konrad-Schmolke et al. 2005; Muncill and Chamberlain 1988; Dachs and Proyer 2002; Willner et al. 2004; Vignaroli et al. 2005). Since the range of accessible experimental temperatures is limited by the relatively low melting temperature of the garnet–clinopyroxene mixtures employed ( $\sim 1,250^\circ\text{C}$  at 1.3 GPa, Vielzeuf et al. 2005a, b) and because of the limited contrast of calcium concentrations, diffusion penetration on laboratory timescales is insufficient for microprobe measurements. Thus the induced diffusion profiles have been measured by analytical transmission electron microscope (ATEM, Vielzeuf et al. 2007).

A summary of garnet compositions studied so far in experimental runs and the diffusivity data obtained for the major divalent cations is given in Table 1 and Fig. 1. Figure 1 compares range of garnet compositions of the present study with previously investigated garnets by projecting onto appropriate ternary end-member diagrams. The data obtained on diffusion rates are not always consistent, especially those produced in different laboratories (Table 1, see also the review of Carlson 2006). Data on Ca diffusion rates remain the most controversial. TC-type experiments on the self-diffusion of  $^{44}\text{Ca}$  in grossular (Schwandt et al. 1996) as well as SOI study in lead to an activation energy that is lower than that of all other divalent cations of smaller ionic radius, although one would expect an opposite tendency (e.g. van Orman et al. 2002). Freer and Edwards (1999) carried out SC diffusion experiments with Ca–Fe diffusion couples containing a

**Table 1** Experimental data for diffusion of divalent cations in garnet

Diffusion couple or tracer	Experimental conditions			Results			Notes <sup>a</sup>	References	
	T (°C)	P (GPa)	Number of runs	f <sub>O<sub>2</sub></sub> (GPa)	Diffusion	Q (kJ/mol)			D° (m <sup>2</sup> /s)
Sps–Alm	1300–1480	2.9–4.3	7	C–O <sub>2</sub> <sup>b</sup>	Fe–Mn <sup>c</sup> in Alm	224	$0.8 \times 10^{-9}$	0.47	SC Elphick et al. (1985)
					Fe–Mn <sup>c</sup> in Sps	238	$1.2 \times 10^{-9}$	0.47	SC Elphick et al. (1985)
Sps–Alm					Fe <sup>2+</sup>	256	$3.1 \times 10^{-9}$		Experimental data of Elphick et al. (1985)
					Mn	201	$2.2 \times 10^{-8}$		--/--
					Mg	250	$2.0 \times 10^{-9}$		--/--
Sps–Alm	1100–1200	1.4–3.5	4	C–O <sub>2</sub>	Fe <sup>2+</sup>	275	$4.66 \times 10^{-8}$	0.56	SC, incorporates data of Loomis et al. (1985) Chakraborty and Ganguly (1992)
					Mg	284	$1.11 \times 10^{-7}$	0.53	--/--
					Mn	253	$5.11 \times 10^{-9}$	0.60	--/--
Alm–Prp	1050–1200	1.8–2.3	6	C–O <sub>2</sub>	Fe <sup>2+</sup>	275	$1.44 \times 10^{-11}$		SC Gerasimov (1987)
					Mg	365	$1.12 \times 10^{-15}$		SC Gerasimov (1987)
Alm–Prp	1057–1432	2.2–4.0	7	C–O <sub>2</sub>	Fe <sup>2+</sup>	274	$3.5 \times 10^{-9}$	0.56	SC Ganguly et al. (1998)
					Mg	254	$4.66 \times 10^{-9}$	0.53	--/--
<sup>24,25</sup> Mg in Prp	750–900	0.2	6	MH	<sup>25</sup> Mg/ <sup>24</sup> Mg	239	$9.8 \times 10^{-9}$		TC Cygan and Lasaga (1985)
<sup>25</sup> Mg in Prp	800–1000	0.0001	19	~QFM	<sup>25</sup> Mg/ <sup>28</sup> Si	294	$0.1 \times 10^{-9}$		TC Schwandt et al. (1995)
<sup>26</sup> Mg in Prp and Alm	1573, 750–850	8.5 and 0.0001	8	~10 <sup>-17.5</sup> bar	<sup>26</sup> Mg	226	$1.82 \times 10^{-10}$	0.80	TC Chakraborty and Rubie (1996)
<sup>44</sup> Ca in Grs	800–1000	0.0001	8	QFM	<sup>44</sup> Ca	155	$7.2 \times 10^{-16}$		TC Schwandt et al. (1996)
Grs–Alm	900–1100	1.5–3.0	17	WI	Ca–(Fe, Mg) <sup>c</sup>	270	$1.0 \times 10^{-6}$	1.12	SC Freer and Edwards (1999)
Grs–(Alm, Prp)	1050–1250	1.3	7	C–O <sub>2</sub>	Ca–(Fe, Mg) <sup>c</sup>	188	$6.6 \times 10^{-14}$		SOI Vielzeuf et al. (2007)

<sup>a</sup> Experimental method: SC sandwiched crystals, TC tracer isotope coating, SOI seed/overgrowth interdiffusion

<sup>b</sup> Graphite–O<sub>2</sub>

<sup>c</sup> Interdiffusion

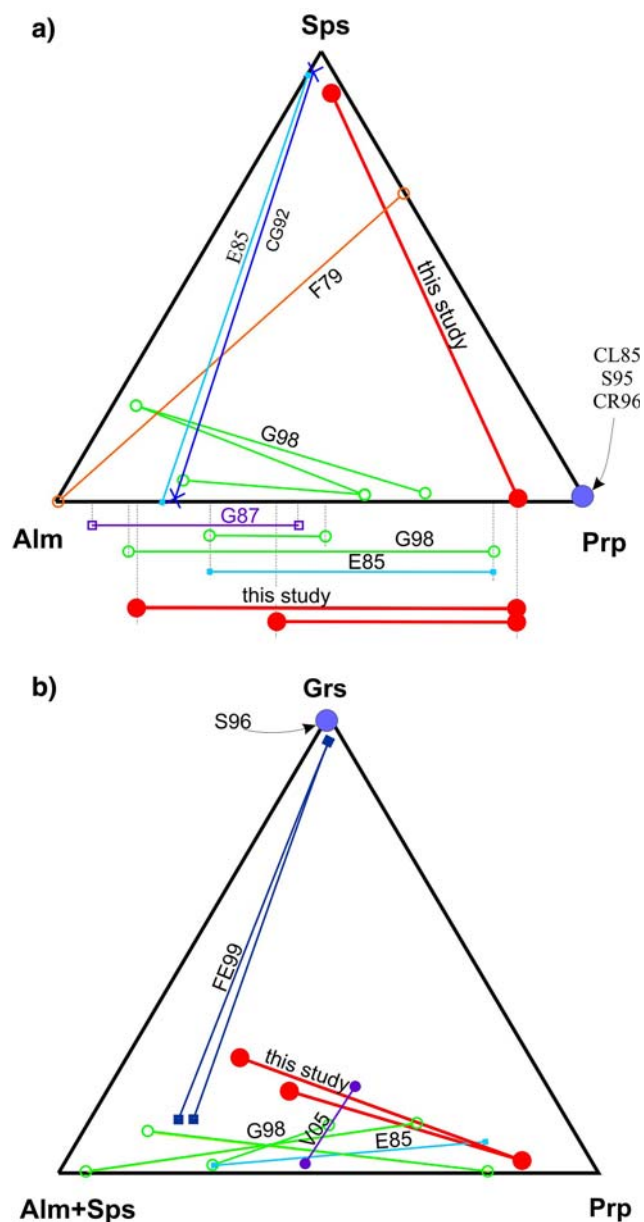


**Fig. 1** Compositions of garnets for which diffusion studies have been carried out. **a** Prp–Alm–Sps and **b** Grs–Alm/Sps–Prp. CG92 Chakraborty and Ganguly (1992), CL85 Cygan and Lasaga (1985), CR96 Chakraborty and Rubie (1996), E85 Elphick et al. (1985), F79 Freer (1979), FE99 Freer and Edwards (1999), G89 Gerasimov (1987), G98 Ganguly et al. (1998), L85 Loomis et al. (1985), S95 Schwandt et al. (1995), S96 Schwandt et al. (1996), V05 Vielzeuf et al. (2005a, b)

relatively high amount of  $\text{Fe}_2\text{O}_3$  (>3 wt%) and  $\text{TiO}_2$  (>1 wt%), and found surprisingly high Ca–Fe interdiffusion coefficients. The diffusivities retrieved by Freer and Edwards (1999) are higher than for other divalent cations of lower ionic radius, and are not consistent with the other experimental data on  $D_{\text{Ca}}$  (Schwandt et al. 1996; Ganguly et al. 1998; Vielzeuf et al. 2007).

Additional information on diffusion rates in garnet comes from the studies of natural samples with well-

constrained temperature–time histories. These data anchor the low-temperature end of the dataset, and extend the range of host compositions well in the quaternary system. Very recently Carlson (2006) demonstrated that all experimental data except for the data sets of Schwandt et al. (1995, 1996) are consistent with his data on natural samples (125 determinations of diffusivities) within  $2\sigma$  errors of  $\pm 0.8 \log_{10}$  units, when the effects of host–garnet composition are taken into account as suggested by Carlson (2006).

## Diffusion experiments

### Starting materials and design of the capsule

Diffusion experiments were carried out primarily with natural garnet crystals close to the Fe, Mn, and Ca end-member compositions embedded in a powder of pyrope close to Mg end-member composition. These compositions were used to retrieve diffusivities for the relatively simple binary systems. The starting materials were augmented by poikiloblastic garnets of intermediate grossular–almandine–pyrope composition from eclogitic rocks, in order to compare the diffusivities in gem-quality crystals close to end-member composition with heterogeneous and inclusion-rich crystals as they commonly occur in metamorphic rocks. The properties and compositions of the garnets used are summarized in Fig. 1 and Tables 2 and 3. Crystals of Sps, Type 1 Alm and Grs are essentially homogeneous and inclusion-free (Table 2). This is in marked contrast to the poikiloblastic and chemically zoned eclogitic garnets of Types 2 and 3 Alm.

The powdered matrix for the experiments was prepared from light pink pyrope from the Dora-Maira massif, Western Alps (Schertl et al. 1991). Gem-quality pieces devoid of visible inclusions were extracted from pyrope crystals 3 cm in diameter. These were milled in an agate mortar to produce fragments 5–70  $\mu\text{m}$  in size. No further separation of the powder according to grain size was made, in order to allow appraisal of any possible effect of grain-boundary diffusion within clusters of different grain sizes. Starting crystals of different size and shape (see below) as well as composition (Table 3) were then embedded in this dry pyrope powder within Pd capsules 8 mm in length, with 3 mm inner diameter and 0.5 mm wall thickness. Special care was taken to prevent atmospheric  $\text{H}_2\text{O}$  from contaminating the starting materials by placing each capsule uncovered in a furnace at 130°C for 2 days or more. After rapid mechanical cold-welding of the capsule, the whole pressure cell was again placed in the furnace for 1–2 days at 130°C. No special control for the oxygen fugacity was attempted, because it is generally considered that graphite-based cell assemblies

**Table 2** Properties of garnets used as starting material

Garnet	Composition	Description	Rock type, origin
Pyrope (Prp)	Alm <sub>12</sub> Prp <sub>83</sub> Grs <sub>4</sub>	Powder consisting of 5–70 $\mu\text{m}$ fragments, pink, gem quality	Pyrope quartzite, Dora-Maira, Western Alps
Spessartine (Sps)	Alm <sub>6</sub> Prp <sub>6</sub> Sps <sub>83</sub> Grs <sub>5</sub>	Cubes of $1 \times 1 \times 1 \text{ mm}^3$ , cubes or slabs $1 \times 1 \times 0.4 \text{ mm}^3$ , light-orange, gem quality	Graphite-mine, Český Krumlov, Czech Republic
Grossular (Grs)	Alm <sub>6</sub> Prp <sub>2</sub> Grs <sub>92</sub>	Cubes of $1 \times 1 \times 1 \text{ mm}^3$ , yellowish, gem quality	Unknown rock, Lake Juko, Coalhila Prov., Mexico
Almandine (Alm <sup>a</sup> )	Alm <sub>81</sub> Prp <sub>14</sub> Sps <sub>2</sub> Grs <sub>3</sub>	Idiomorphic or spherical crystals, reddish, gem quality	Dacite, Cerro del Hoyazo, ~3 km W Níjar (S. Spain)
Almandine (Alm <sup>b</sup> )	Alm <sub>45–47</sub> Prp <sub>32–36</sub> Sps <sub>1</sub> Grs <sub>18–20</sub>	Idiomorphic crystals, brownish-red, euhedral, poikiloblastic cores with numerous mineral inclusions	Eclogite, Cordillera, Canada
Almandine (Alm <sup>c</sup> )	Alm <sub>54</sub> Prp <sub>13–22</sub> Sps <sub>0–9</sub> Grs <sub>18–24</sub>	Slab of 0.4 mm width, radially oriented, brownish-red, numerous mineral inclusions (predominantly quartz) in the core	Eclogite, Caucasus, Russia

**Table 3** Representative microprobe analyses of initial garnets

	Pyrope (Prp)	Grossular (Grs)	Spessartine (Sps)	Almandine (Alm <sup>a</sup> )	Almandine (Alm <sup>b</sup> ) <sup>A</sup>	Almandine (Alm <sup>c</sup> ) <sup>A</sup>
SiO <sub>2</sub>	42.62	39.05	36.73	36.56	38.93	37.98
Al <sub>2</sub> O <sub>3</sub>	24.44	19.70	20.65	21.03	22.09	21.88
FeO	6.48	2.59	2.81	37.28	22.01	25.15
MnO	0.11	0.12	35.91	0.82	0.26	0.41
MgO	24.08	0.74	1.85	3.36	9.61	6.47
CaO	1.68	37.33	1.71	1.08	6.61	7.67
Sum	99.40	99.53	99.65	100.13	99.51	99.56

<sup>A</sup> Rim compositions**Table 4** Experimental conditions of the diffusion series

Run	Single crystals <sup>A</sup>	Powder	<i>T</i> (°C)	<i>P</i> (GPa <sup>B</sup> )	<i>t</i> (h)	Comments
DB1	Alm <sup>a</sup> , Sps, Grs, Alm <sup>b</sup> , Alm <sup>c</sup>	Prp	1,300	3.0 (2.6)	96	Single capsule
DB4	Alm <sup>a</sup> , Sps, Grs, Alm <sup>b</sup> , Alm <sup>c</sup>	Prp	1,150	3.0 (2.6)	480	Single capsule
DB5	Alm <sup>a</sup> , Sps	Prp	1,400	3.8 (3.2)	24	Two capsules, one with graphite added
DB6	Alm <sup>a</sup> , Sps, Alm <sup>b</sup> , Alm <sup>c</sup>	Prp	1,070	2.2 (1.9)	501	Single capsule

<sup>A</sup> See Tables 2 and 3 for details and abbreviations<sup>B</sup> Nominal pressure. In parentheses—pressure with friction correction (–15%)

constrain the  $\log(f_{\text{O}_2})$  in the sample to lie between the QFM buffer and QFM-2 (Patiño Douce and Harris 1998). However, in one experiment (see DB5 in Table 4), two capsules were run simultaneously, with a 1 mm graphite platelet added to one of them, in order to check effect of conjugate variations of  $f_{\text{O}_2}$  and  $f_{\text{CO}_2}$  on the diffusivity of cations in garnet. After the runs, the capsules were embedded in epoxy and carefully sectioned (see below). The sectioned crystals were then separated from the epoxy with chloroform, cleaned in ethanol, and washed for 20 min in distilled water in an ultrasonic bath.

Different crystal shapes and different packing designs in the Pd capsules were tested in order to optimize the design of the capsule, such as to attain the best preservation of the crystals, to simplify their recovery after the run, and to allow precise control and interpretation of the sectioning procedure. Natural Alm<sup>a</sup> and Alm<sup>b</sup> crystals are either euhedral or rounded in shape (Table 2). These garnets are smaller than the inner diameter of the capsules used and thus these crystals were used without further preparation of their natural surfaces. Preliminary SEM study of the same garnets revealed that they possess plenty of domains with

flat surfaces appropriate for interdiffusion study. All other crystals were sectioned with a micro-saw to slabs of 0.4 mm thickness or to cubes approximating ( $\sim 1 \times 1 \times 1$  mm) (Table 2). After sawing, each sample was ground on both sides on the diamond bearing “bronze plates” starting from 46  $\mu\text{m}$  diamond grit, than 25 and finally 15  $\mu\text{m}$  diamond paste. Then the sample was polished on lead plates with a 1  $\mu\text{m}$  diamond spray, followed by polishing on OPA-suspension. Samples were finally cleaned in ethanol and rinsed ultrasonically. Precise knowledge of the shape and starting-grain diameter is crucial, because the extent of the interdiffusion zone in garnets after the run will be influenced strongly by the sectioning procedure. As shown in Fig. 2, the width of this zone will be a minimum and realistic only when the grain surface is truly normal to the surface of the section, i.e. when garnet is cut through its centre. Any other sectioning of a spherical garnet will lead to inclination of the grain surface, accompanied by artificial effects such as a decrease of the grain size and an increase of the interdiffusion zone. Geometrical constrains show that an artificial decrease of the grain size of  $\sim 30\%$  due to imprecise sectioning leads to an inclination angle with the crystal surface of  $\sim 45^\circ$ , and an artificial increase in the interdiffusion zone of  $\sim 40\%$  (Fig. 2). The corresponding deviations in the evaluated diffusion coefficients can be significant. We minimized the “sectioning effect” in our runs by considering only those garnets where the dimension of the section was at least 80% of the true garnet size, thus corresponding to a deviation angle of less than  $35^\circ$  and an artificial modification of the interdiffusion zone of less than 20%. We attained these relatively low values by meticulous control of both the initial packing procedure of the starting garnets (Fig. 3) and of capsule orientation at all stages of handling, so as to optimize sawing of the capsule close to the centres of spherical grains and perpendicular to the surfaces of cubes and slabs.

#### Apparatus and experimental conditions

Experiments were performed in end-loaded, solid-medium piston-cylinder apparatus (Fockenberg 1998; Perchuk et al. 2005) with 12.7 mm diameter “talc-glass” assemblies (Fig. 4). The temperature (1,070–1,400°C) and nominal pressure (2.2–3.8 GPa) conditions of the experiments were well within the stability fields of the garnets of chosen compositions. The pressure, temperature and run durations of the experiments were chosen so as to achieve an expected 10  $\mu\text{m}$  length for the Fe–Mg interdiffusion profile. The calculated diffusion profiles were retrieved with the DXL program of Perchuk and Gerya (2005). We initially used the most recent diffusion coefficients available (Ganguly et al. 1998) and refined these during the progress of the study. The chosen length of 10  $\mu\text{m}$  is sufficient for

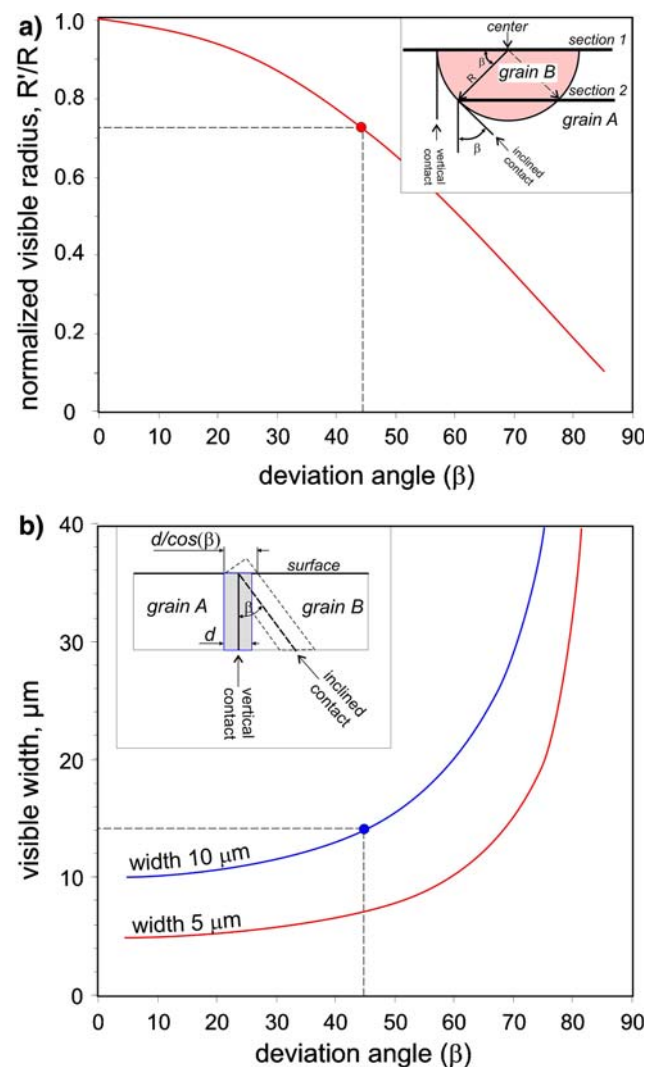


**Fig. 2** Geometric analysis of the sectioning effect. **a** Dependence of the  $\beta$  deviation angle on the normalized visible radius. The inset shows half of a spherical grain and the location of two cross sections—one ideally through the grain centre, and a second one that produces a deviation angle with the interface of  $45^\circ$ . These are the optimum (section 1) and worst-case (section 2) possibilities during of a spherical garnet during preparation of the sample. The observed diameter of the grain in section 2 is equal to  $2 \times R \times \cos(\beta)$ ; **b** observed width of an interdiffusion zone of actual width of 5 or 10  $\mu\text{m}$ , respectively, as function of the deviation angle. The inset shows two grains, their vertical contact (solid line), interdiffusion zone (gray), inclined contact (dashed line) and corresponding observed increase of the interdiffusion zone. The point indicates the effect of a  $45^\circ$  inclination angle is. Symbols  $\beta$  inclination angle,  $R$  radius of the grain,  $d$  thickness of the interdiffusion zone. See text for further details

electron microprobe profiling and needs no correction on convolutions, as shown by our calculations with the method of Ganguly et al (1988). We did not carry out any time series studies, based on experience gained in previous electron-microprobe-related studies of diffusivity in garnet (Elphick et al. 1985; Chakraborty and Ganguly 1992;

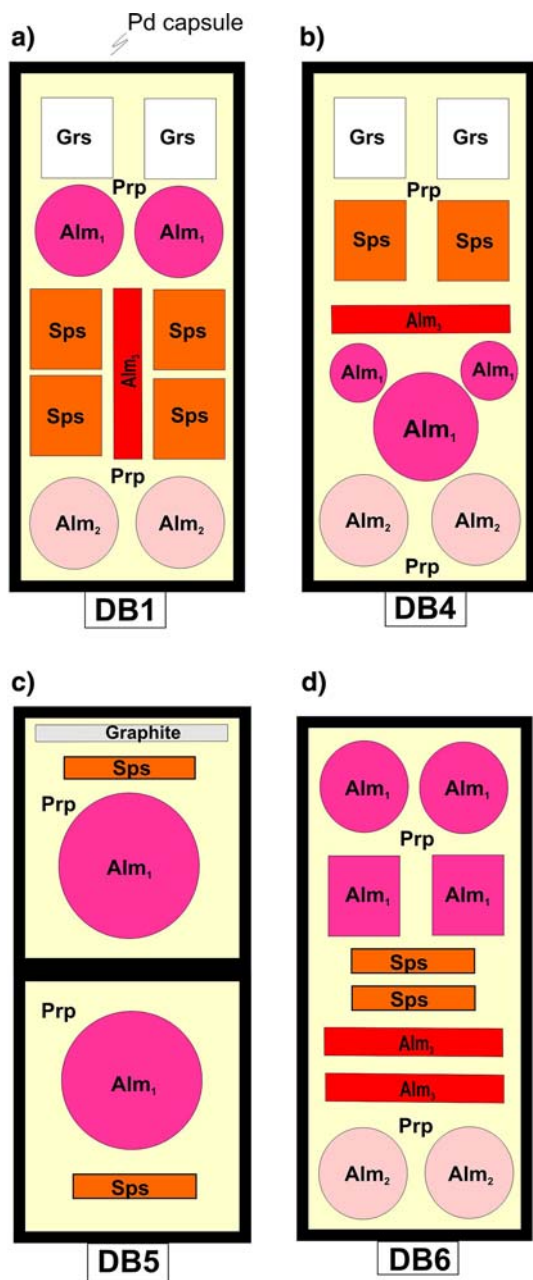


**Fig. 3** Schematic designs of the capsules in different runs: **a** DB1, **b** DB4, **c** DB5, **d** DB6. Note, there are two capsules in run DB5 (c) and upper contains graphite blade

Ganguly et al. 1998) and the convincing arguments of Ganguly et al. (1998, p. 176) on this topic.

Temperature was measured and controlled with W-WRe<sub>3</sub>/W-WRe<sub>25</sub> thermocouples to ±3°C and monitored continuously with an internal ice-point compensator, connected to a computer for data acquisition and storage. The controller has a manual mode that we used at the start of each experiment. The capsule was emplaced in the area of the minimal thermal gradient calculated using the experimentally tested program of Schilling and Wuender (2004).

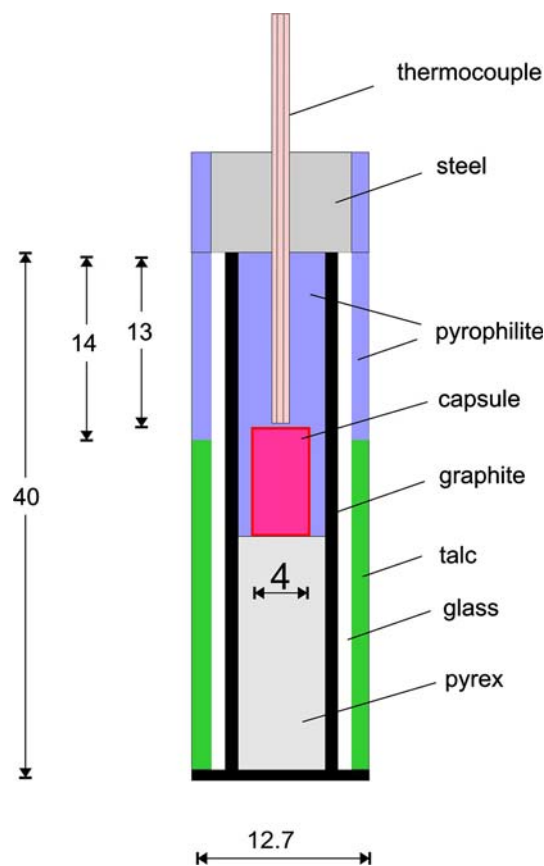


**Fig. 4** Schematic illustration of the pressure cell used in the diffusion experiments. Dimensions are in millimeters. See text for details

According to our calculations with this program, the hot spot of the pressure cell was displaced towards the steel base plug (cf. Pickering et al. 1998) and the temperature close to the center of the 8 mm capsule (initial size before compression, see below) was 41–46°C (runs at 1,070 and 1,400°C, respectively) higher than the thermocouple reading, a result that is consistent with the experimental data of Watson et al. (2002, their Fig. 10) and Schilling and Wuender (2004, their Fig. 9), as well as the numerical modeling of Herlund et al. (2006, their Fig. 4). Accordingly, the deviation of the diffusion coefficient at the hottest part of the capsule close to its centre will be of about 0.3 log<sub>10</sub> units compared to the coldest area of the capsule (close to the tip of the thermocouple).

The oil pressure was measured at the gate of the piston ram by an electronic pressure transmitter, and monitored by a controller. The controller was also connected to the computer, and measured pressures were recorded continuously every minute. Pressure was kept constant during the long term experiments to within ±50 MPa of the nominal value. The correction for friction in the talc-glass assembly is normally considered to be -15% (Takahashi 1986; Chakraborty and Ganguly 1992). To minimize problems

during loading and unloading of the cell, and to maintain garnets within their stability fields, the run conditions were approached very slowly in  $\sim 2$  h by manual control of heating and compression up to  $\sim 600^\circ\text{C}$  and 1 GPa (well outside the brittle behavior of garnet), followed by instrument-controlled linear heating and compression. All the experiments were slowly cooled and depressurized over  $\sim 1.5$  h. Systems of parallel cracks in garnet perpendicular to the elongation of the capsule appeared during depressurization of the assembly, as already pointed out Perchuk et al. (2005) who observed parallel cracks which crosscut quenched melt inclusions in garnet in the runs of very similar design (their Fig. 2e, f). The extracted capsules were emplaced in epoxy, cut along the capsule length close to the centers of the spherical garnets and then polished. Some fragments were investigated further by sectioning across the capsule and polishing.

### Run products and electron microprobe profiling

Capsules were generally shortened by about 25% to  $\sim 6$  mm after the run because of compression of the pyrope powder. We did not observe distortion of the furnace in it in the vicinity of the capsule suggesting that local hot spots in the furnace were lacking. Spherical and idiomorphic crystals of  $\text{Alm}^{\text{a}}$  garnet were commonly well preserved during the runs (Fig. 5a). Deformation of the other types of garnet was dependent on their position within the capsule. The small slabs of garnet are the most vulnerable to deformations, often being bent or crushed against other

garnet crystals (Figs. 6, 7). Collision was typical for slabs with vertical positioning (e.g. Fig. 6), while horizontal slabs were either bent or undeformed. Deformation of poikiloblastic  $\text{Alm}^{\text{b}}$  garnets occurred locally in some “collision zones” and was enhanced by the partial melting that weakened the crystals. Local areas garnet host modification ( $\text{Alm}^{\text{b}}$ ,  $\text{Alm}^{\text{c}}$ ) due to dehydration partial melting of inclusions (Perchuk et al. 2005) did not rich inclusion-free areas of interdiffusion profiles. Cubes preserve their original shape in protected domains (Figs. 5b, 6). In contrast to the experiments with sintered garnet + clinopyroxene powder of Vielzeuf et al. (2007), overgrowths enveloping initial crystals were not observed. There is, however, a reaction zone between grossular and sintered pyrope consisting of Ca–Mg garnet. The inner part of the reaction zone is rather homogeneous in composition and contains tiny remnants ( $<5 \mu\text{m}$ ) of the initial grossular. The outer part is free of such remnants and shows a gradual decrease of Ca and increase of Mg towards the contact with pyrope. Both contacts of the reaction-zone garnet with pyrope and grossular are sharp, but so irregular in shape that it was impossible to find a location appropriate for electron microprobe profiling across the interdiffusion zone. For this reason, no attempt was made to obtain diffusion coefficients for the grossular-pyrope diffusion couple in this study.

Backscattered electron images (BSE) reveal different types of contacts between single garnets and the surrounding sintered matrix. Some of the contacts are simple without any fracturing and grain-boundary channeling (Fig. 5a). Microprobe profiles of such domains have been

**Fig. 5** Example of well-preserved garnets after the runs. **a** DB1—spherical almandine ( $\text{Alm}^{\text{a}}$ ). Reflected light image. Inset X-ray map of Mg (blue low Mg, red high Mg) indicating that contact between almandine and pyrope is free of channeling; **b** DB1—cubes of grossular in pyrope; **c** DB6—capsule with crystals of different shape

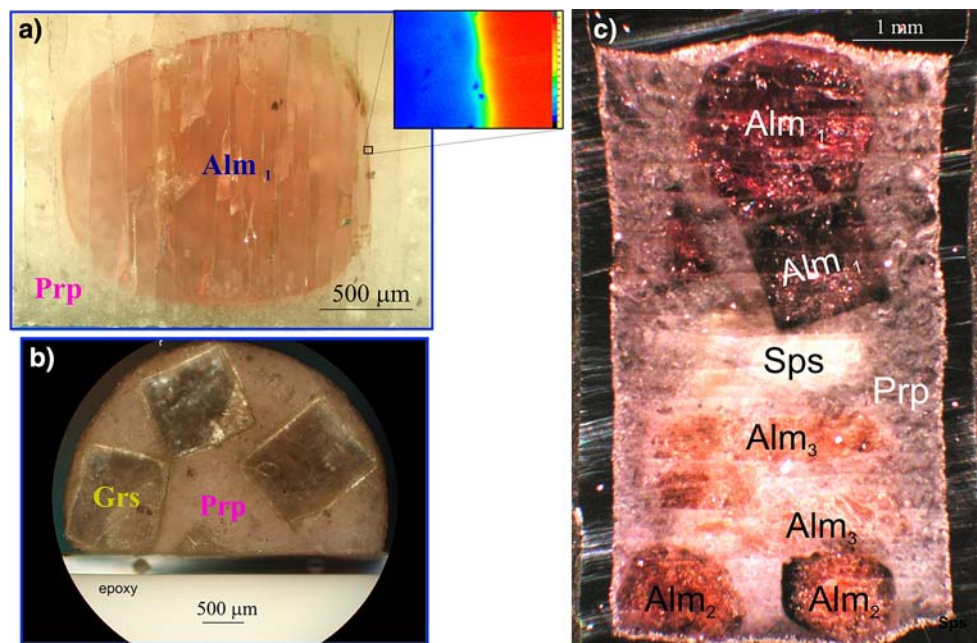


**Fig. 6** X-ray maps of the capsule after run DB1 at 1,300°C, 2.6 GPa for 96 h: **a** Mg. Rim around grossular corresponds to chemical interface reaction; **b** Fe. *Circles* collision zone between slab and single crystal. *Arrows* local area of unusually intensive channeling owing to grain-boundary diffusion. Note deformation of the type 3 Alm slab and partial melting of inclusions within type 2 Alm (cf. Perchuk et al. 2005). The images have been treated with the XMAP program of H.-J. Bernhardt

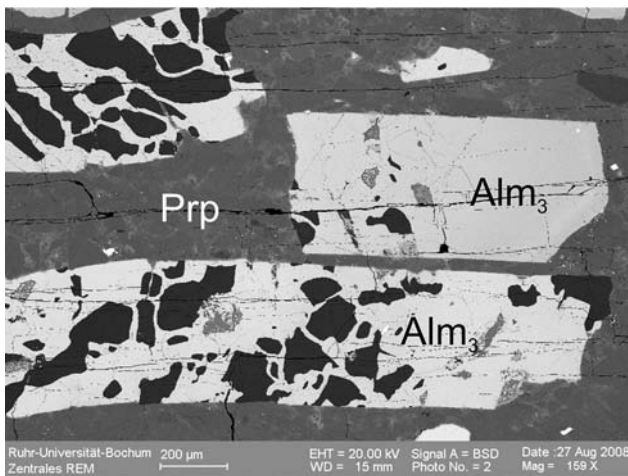
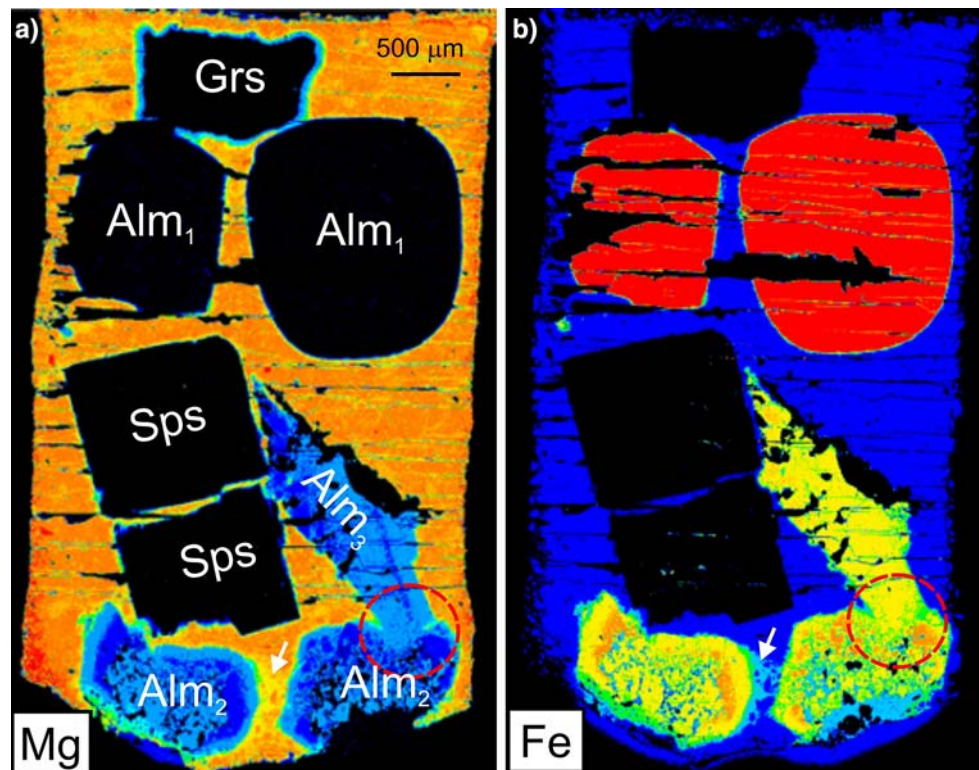


**Fig. 7** Banded slabs of eclogitic garnet ( $\text{Alm}^c$ ) filled with inclusions. Run DB6 at 1,070°C, 1.8 GPa for 501 h. BSE image

chosen normal to the flat interface. Quite often the contacts are affected by preferential channeling of diffusion along grain interfaces (Fig. 6). The degree and scale of channeling varies from one domain to another. We assume that this is generally dependent on the initial grain size of the powder along the contact. The larger the initial grains are the less significant and less developed is the network of grain boundaries and thus the matrix is less affected by channeling. This also supports our strategy to use pyrope powder of variable grain size—the finer powder is

necessary for a better packing, whereas the coarser ( $>50 \mu\text{m}$ ) leads to the formation of simple interdiffusion zones. Electron microprobe profiles from the domains affected by grain-boundary channeling have also been used in a qualitative way to check the effect of “leakage” of cations from the interdiffusion zone along the grain boundaries. The average length of grain-boundary penetration commonly does not exceed tens of micrometers. There are, however, rare domains related to partial melting, where grain-boundary diffusion penetrated for distances of more than  $100 \mu\text{m}$  (Fig. 6).

The induced diffusion profiles were measured by step and beam scanning using a 4-spectrometer electron microprobe CAMECA SX 50 at the Ruhr-University in Bochum, with an accelerating voltage of 15 kV, an incident beam current of 15 nA and 20 s counting time per element. Concentrations of the common elements in silicate garnets (Ca, Mg, Fe, Mn, Al, and Si) were determined. A minimum beam spot size of  $0.7 \mu\text{m}$  was used. Well-characterized natural and synthetic minerals were used as standards.

BSE imaging was used each time to find a suitable section of the interface. Several sets of line scans in different sections of each single garnet crystal and sintered matrix were measured with full quantitative WDS analyses (24–45 profiles per sample). The analyses were employed for profiling with steps of  $0.5\text{--}1.0 \mu\text{m}$  across the boundary. Relatively long profiles ( $>8\text{--}10 \mu\text{m}$ ) were induced in the

diffusion couples close to end-member compositions. Such profiles were quantified using the stage-scanning mode with a step of 1  $\mu\text{m}$ . A beam scanning mode with steps of 0.5  $\mu\text{m}$  was applied for traverses across contacts of those eclogitic garnets ( $\text{Alm}^{\text{b}}$ –Prp and  $\text{Alm}^{\text{c}}$ –Prp) where the interdiffusion zones were found to be relatively narrow (<6  $\mu\text{m}$ ). Small-step traverses permit minimization of spatial averaging in the electron microprobe analysis by deconvolution procedure. For deconvoluted profiles we applied the approach of Ganguly et al. (1988), with an error SD of the intensity distribution of X-rays of  $\varepsilon = 0.58 \mu\text{m}$  for step size of 0.5  $\mu\text{m}$ . The  $\varepsilon$  value was established by Ganguly et al. (1988) for an electron microprobe of type Cameca SX-50 for ranges of beam current between 10 and 50 nA, and for an accelerating voltage between 11 and 20 kV, i.e. well within our analytical conditions. Convolution effects were significant for Ca in all the runs and also for Fe and Mg in  $\text{Alm}^{\text{b}}$ –Prp and  $\text{Alm}^{\text{c}}$ –Prp diffusion couples in run DB6 (Fig. 8). The other profiles were sufficiently long (>12  $\mu\text{m}$ ) to allow deconvolution analysis to be neglected. Indeed, errors owing to the convolution effect for these profiles are below 7% (Ganguly et al 1988, Eq. 20) and original and deconvoluted profiles become graphically indistinguishable (e.g. Ganguly et al 1988, Fig. 5b). Note that the effect of convolution may be removed using the equation  $D = D_c - \varepsilon^2/2t$  (Eq. 19, Ganguly et al. 1988), where  $D_c$  is the diffusion coefficient retrieved from the convoluted diffusion profile,  $\varepsilon$  is the standard deviation of the Gaussian error function of the excited sample volume, and  $t$  is time.

The highest temperature diffusion profiles in  $\text{Alm}^{\text{a}}$ –Prp diffusion couple show asymmetry: typically the compositional curves are steeper in pyrope and flatter in almandine (Fig. 9). This implies that the interdiffusion is dependent on composition and increases with higher Fe contents. However, this asymmetry disappears at lower temperatures

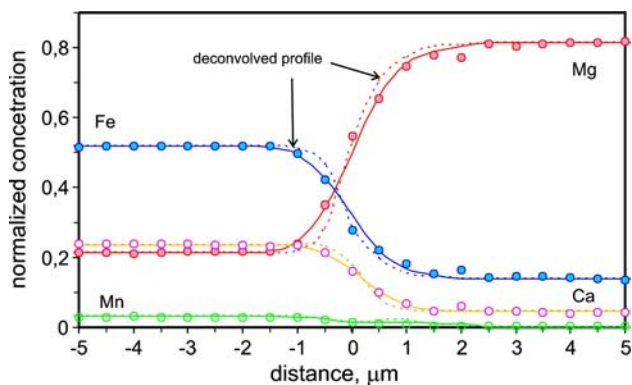


**Fig. 8** Deconvolution of electron microprobe profile induced in the  $\text{Alm}^{\text{c}}$ –Prp diffusion couple in the run DB6 at 1,070°C, 1.8 GPa for 501 h. Dots points of microprobe analyses, dashed lines deconvoluted profile, solid lines convoluted profile. See text for details

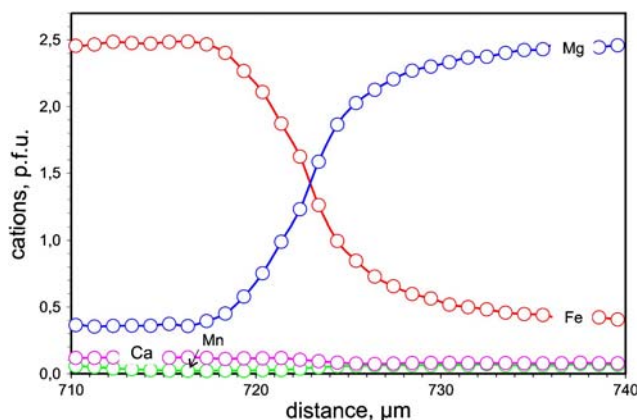


**Fig. 9** Asymmetric microprobe profile induced in  $\text{Alm}^{\text{a}}$ –Prp diffusion couple in the run DB5 at 1,400°C, 3.2 GPa for 24 h

either due to the approaching the diffusion coefficients of the two species in the Fe–Mg join and/or the masking of the asymmetry in short profiles. Mn and Mg in spessartine–pyrope diffusion couples reveal no obvious asymmetry, suggesting very similar diffusivities in the whole experimental range.

## Modeling and results

The experimentally induced profiles in spessartine–pyrope and almandine ( $\text{Alm}^{\text{a}}$ ,  $\text{Alm}^{\text{b}}$  and  $\text{Alm}^{\text{c}}$ )–pyrope diffusion couples were used to obtain the self-diffusion coefficients  $D_i$  of Mg, Mn, Fe and Ca. Here we define the self-diffusion coefficient,  $D_i$ , of an element as the diffusion coefficient of the element itself in response to its own concentration gradient (Ganguly et al. 1998).

The mathematical technique of treating multicomponent diffusion is well established (e.g. Onsager 1945; Toor 1964; Lasaga 1979). We assume that garnet is an effectively ideal solution at the experimental conditions (Chakraborty and Ganguly 1992), and thus no correction for thermodynamic effects was incorporated in our computations.

In the case of multicomponent diffusion in a given mineral, the cation fluxes will depend on a linear combination of all the cation gradients, with the linear coefficients given by the diffusion matrix,  $D_{ij}$ . If the diffusion coefficients,  $D_{ij}$ , are compositionally dependent, the Ficks–Onsager relation (Onsager 1945) has the following form in one dimension,

$$\frac{\partial C_i}{\partial t} = \frac{\partial}{\partial x} \sum_{j=1}^{n-1} D_{ij} \left( \frac{\partial C_j}{\partial x} \right) \quad (1)$$

where  $C_i$  is a mole fraction of the component  $i$  in a  $n$ -component system,  $x$  is the distance. According to

Lasaga (1979), the diffusion matrix in complex silicates can be evaluated as follows,

$$D_{ij} = D_i \delta_{ij} - \left[ \frac{D_i z_i z_j C}{\sum_{k=1}^n z_k^2 C_k D_k} \right] (D_j - D_n) \quad (2)$$

where  $\delta_{ij} = 0$  if  $i \neq j$  and 1 if  $i = j$ , the  $n$ th element is treated as a dependent component. Self-diffusion coefficients,  $D_{i(j,k)}$ , have been calculated using the following Arrhenius relationship (Chakraborty and Ganguly 1992)

$$D_i = D_i^0 \exp\left(\frac{-(Q_i + P\Delta V_i)}{RT}\right) \left(\frac{f_{O_2}}{f_{O_2}^{gr}}\right)^{1/6}, \quad (3)$$

where  $D^0$  is a pre-exponential factor,  $Q_i$  is the activation energy at 1 bar,  $\Delta V_i$  is the activation volume (according to Chakraborty and Ganguly 1992), and  $f_{O_2}^{gr}$  is the oxygen fugacity in the graphite–oxygen equilibrium.

In the case of analytical solution, off-diagonal terms in Eq. 1 prevent treatment of the problem as a simple diffusion equation. However, the problem is commonly solved by introduction of a new set of ‘generalized’ or ‘eigen’ components (e.g. Lasaga 1979), which reduce the system of equations to a set of independent (binary) diffusion equations that can be solved by analytical or numerical methods.

In this study, the set of coupled diffusion equations for a four-component system was solved numerically using the DXL program of Perchuk and Gerya (2005), which is based on conservative finite-differences (FD) schemes for an irregular grid. Following Loomis et al. (1985), the DXL program was tested by comparison with the analytical solution for a diffusion coefficient strongly dependent on composition (Crank 1975, p. 118). As demonstrated by Perchuk and Gerya (2005, their Fig. 6), the numerically simulated profile is in excellent agreement with the analytical values of Table 7.5 in Crank (1975, p. 386).

Self-diffusion coefficients of Mg, Fe, Mn and Ca have been retrieved by numerical simulations with the DXL program of the experimentally induced diffusion profiles in Alm<sup>a</sup>–, Alm<sup>b</sup>–, Alm<sup>c</sup>–Prp, and Prp–Sps diffusion couples. Although the diffusion fluxes operated mainly in terms of 2 or 3 exchange components we have, however, performed four-component diffusion modeling (Fig. 10). This simplifies comparison of our data with previous studies (e.g. Elphick et al. 1985; Loomis et al. 1985; Chakraborty and Ganguly 1992; Ganguly et al. 1998). In addition, we have checked the role of minor components on the diffusivity of the components with major compositional differences (e.g. effect of Fe in Prp–Sps diffusion couple), and found this effect to be negligible. The results of the computations are summarized in Table 5. Three or more profiles were typically measured on each diffusion couple. The average of

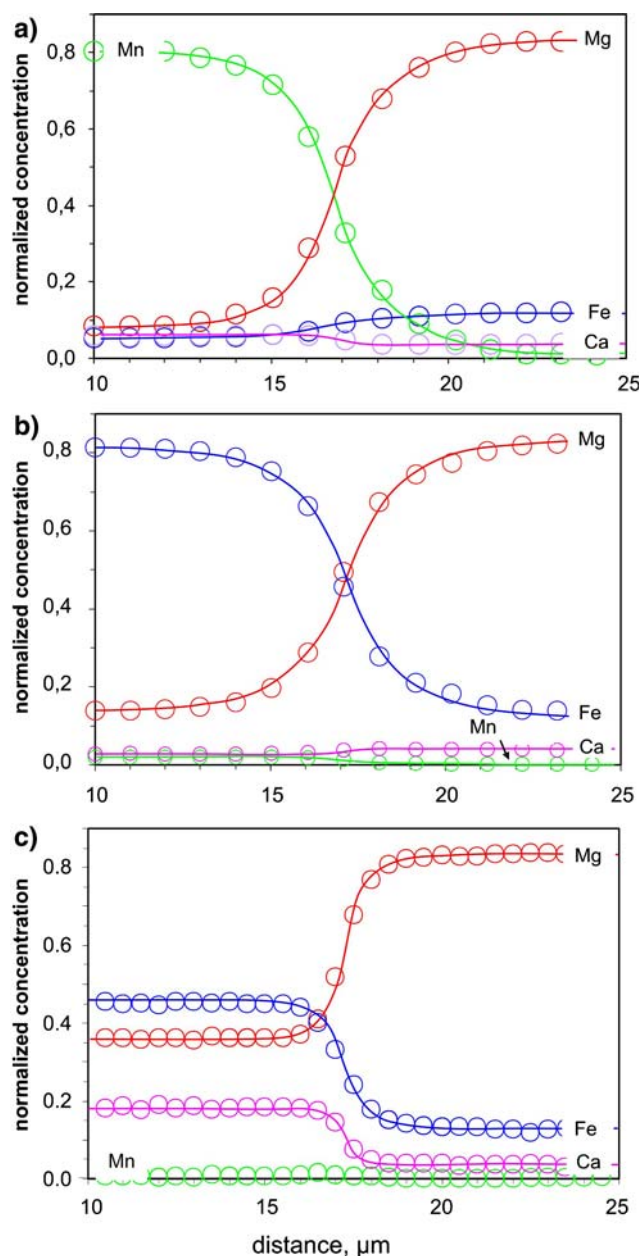


**Fig. 10** Measured (circles) and simulated (lines) diffusion profiles in different diffusion couples at 1,070°C, 1.9 GPa for 501 h. **a** Sps–Prp diffusion couple. Self-diffusion coefficients ( $m^2/s$ ) of the fitted profile are Mg  $5.06 \times 10^{-19}$ , Fe  $7.08 \times 10^{-19}$ , Mn  $9.27 \times 10^{-19}$  and Ca  $4.93 \times 10^{-20}$  ( $D_{Ca}$  and  $D_{Fe}$  are not significant); **b** Alm<sup>a</sup>–Prp, Mg  $9.73 \times 10^{-19}$ , Fe  $9.91 \times 10^{-19}$ , Mn  $6.49 \times 10^{-19}$  and Ca  $4.93 \times 10^{-20}$  ( $D_{Ca}$  and  $D_{Mn}$  are not significant); **c** Alm<sup>c</sup>–Prp, deconvolved profile, Mg  $1.39 \times 10^{-19}$ , Fe  $1.61 \times 10^{-19}$ , Mn  $2.63 \times 10^{-19}$  and Ca  $6.17 \times 10^{-20}$  ( $D_{Mn}$  is not significant)

the profiles that had no irregularities caused by grain-boundary diffusion (see below) was taken to be the diffusivity at the given set of conditions (Table 6). To minimize sectioning effect in spherical garnets (Fig. 2), only the two shortest profiles were taken in each run. Figure 10 illustrates representative examples of the experimental and

**Table 5** Summary of self-diffusion coefficients for specific experimental run conditions

Run	Diffusion couple	<i>T</i> (°C)	<i>P</i> (GPa)	<i>t</i> (h)	<i>D</i> <sup>A</sup> (10 <sup>-18</sup> m <sup>2</sup> /s)			
					Mg	Fe	Mn	Ca
DB1	Alm <sup>a</sup> -Prp	1,300	2.6	96	29.3	10.6		
	Alm <sup>bA</sup> -Prp	1,300	2.6	96	6.65	7.45		0.863
	Alm <sup>c</sup> -Prp	1,300	2.6	96	6.98	5.59		0.743
	Sps-Prp	1,300	2.6	96	27.9		28.9	
DB4	Alm <sup>a</sup> -Prp	1,150	2.6	480	1.26	0.902		
	Alm <sup>b</sup> -Prp	1,150	2.6	480	1.15	9.84		0.145
	Sps-Prp	1,150	2.6	480	1.64		3.48	
DB5	Alm <sup>a</sup> -Prp	1,400	3.2	24	118	99.1		
	Alm <sup>a</sup> -Prp <sup>B</sup>	1,400	3.2	24	96.7	47.9		
	Sps-Prp	1,400	3.2	24	84.1		43.0	
	Sps-Prp <sup>B</sup>	1,400	3.2	24	88.3		73.7	
DB6	Alm <sup>a</sup> -Prp	1,070	1.9	501	0.895	0.991		
	Alm <sup>bA</sup> -Prp	1,070	1.9	501	0.371	0.295		0.0493
	Alm <sup>cA</sup> -Prp	1,070	1.9	501	0.126	0.177		0.0854
	Sps-Prp	1,070	1.9	501	0.662		0.927	

<sup>A</sup> Alm<sup>b</sup> and Alm<sup>c</sup> are poikiloblastic and chemically zoned garnets

<sup>B</sup> Run with graphite

**Table 6** Arrhenius parameters (Eq. 1) for divalent cations in different diffusion couples

Diffusion couple	Component	<i>D</i> <sup>o</sup> (m <sup>2</sup> /s)	<i>E</i> <sup>a</sup> (kJ/mol)	Δ <i>V</i> <sup>aA</sup> [J/(mol bar)]	<i>R</i> <sup>2</sup>
Sps-Prp	Mn	1.51 <sup>+1.64</sup> <sub>-0.41</sub> × 10 <sup>-8</sup>	249.3 <sup>+33.8</sup> <sub>-18.0</sub>	0.60 ± 0.29	0.9917
	Mg	7.79 <sup>+12.00</sup> <sub>-3.91</sub> × 10 <sup>-7</sup>	302.3 <sup>+28.0</sup> <sub>-10.6</sub>	0.53 ± 0.30	0.9984
Alm <sup>a</sup> -Prp	Fe <sup>2+</sup>	9.11 <sup>+9.69</sup> <sub>-0.64</sub> × 10 <sup>-8</sup>	277.6 <sup>+60.6</sup> <sub>-42.8</sub>	0.56 ± 0.29	0.9648
	Mg	9.64 <sup>+3.15</sup> <sub>-1.52</sub> × 10 <sup>-7</sup>	304.3 <sup>+43.1</sup> <sub>-24.4</sub>	0.53 ± 0.30	0.9912
Alm <sup>b,c</sup> -Prp	Fe <sup>2+</sup>	5.06 <sup>+11.58</sup> <sub>-0.62</sub> × 10 <sup>-7</sup>	313.4 <sup>+43.1</sup> <sub>-24.4</sub>	0.56 ± 0.29	0.9789
	Mg	1.13 <sup>+2.42</sup> <sub>-0.88</sub> × 10 <sup>-6</sup>	322.8 <sup>+56.2</sup> <sub>-35.1</sub>	0.53 ± 0.30	0.9822
	Ca	8.37 <sup>+5.90</sup> <sub>-3.36</sub> × 10 <sup>-10</sup>	255.7 <sup>+45.2</sup> <sub>-28.5</sub>	0.60 ± 0.29	0.9895

Uncertainties (1σ) were determined from the linear regression

<sup>A</sup> Data of Chakraborty and Ganguly (1992)

fitted diffusion profiles for different types of diffusion couples.

Self-diffusion coefficients of three diffusion couples in individual runs are plotted as a function of inverse temperature in an Arrhenius diagram in Fig. 11. The Arrhenius parameters in Eq. 3 obtained by the linear regression are listed in Table 6. The uncertainties of the kinetic parameters represent ±1σ values arising from (a) scatter of the experimental points in the *P*-*T* space (Loomis et al. 1985; Chakraborty and Ganguly 1992; Ganguly et al. 1998) and (b) uncertainties of temperature in the capsule, which result from +46°C evaluated from thermal modeling and the ±3°C uncertainty of the thermocouple (Fig. 11). Values for the self-diffusion coefficients of Fe and Mg in the Alm-Prp diffusion couples are very close both poikilitic and gem-quality crystals provide very close values (Table 6, Fig. 11). The self-diffusion coefficient of Ca was retrieved only from the couple with poikilitic garnet and shows that this cation diffuses slower than Fe and Mg (Fig. 11). Note, the *D*<sub>Ca</sub> may be comparable to the self-diffusion coefficients of the other divalent cations under metamorphic

conditions (<900°C), because of the lower activation energy (assuming no change of diffusion mechanism, Ganguly et al. 1998). A relatively low activation energy for *D*<sub>Ca</sub> in grossular and Ca-(Fe, Mg) interdiffusion coefficient has been earlier suggested by Schwandt et al. (1995) and Vielzeuf et al. (2007), respectively.

## Discussion

### Comparison with previous data

Available experimental data on divalent cations diffusivities in garnet are based on the studies carried out in different laboratories using different experimental approaches at a variety of oxygen fugacities, compositional and experimental *P*-*T*-*t* ranges as summarized above (Table 1, Fig. 1; see also Jaoul and Sautter 1999; Béjina et al. 2003; Carlson 2006; Vielzeuf et al. 2007). Comparison of such different data is commonly performed on the basis of pressure and oxygen fugacity normalization (e.g. Ganguly

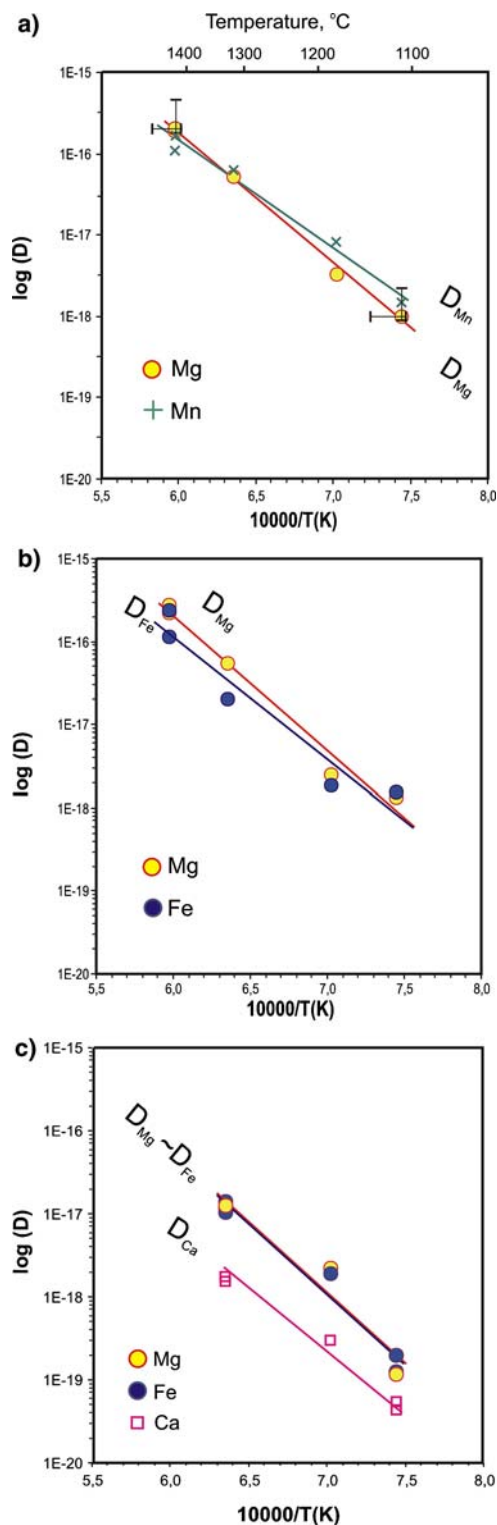


**Fig. 11** Arrhenius plot of experimental self-diffusion coefficients normalized to a pressure of 1 GPa. **a** Spessartine–pyrope diffusion couple; **b** almandine–pyrope; **c** eclogitic garnets–pyrope. Error bars illustrate SD for  $D_{\text{Mg}}$  at 1,070 (lowest) and 1,400°C (highest) originated from uncertainties of  $T$  and  $f_{\text{O}_2}$

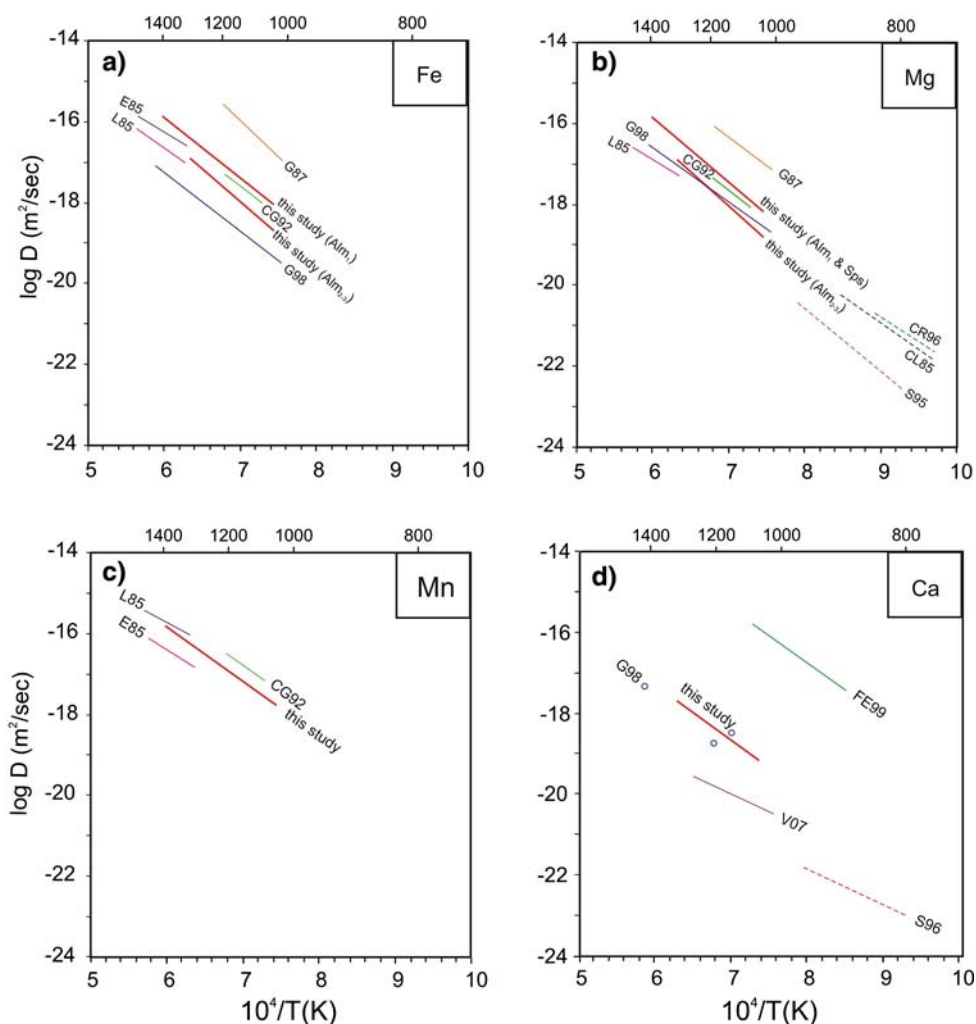
et al. 1998). We used the experimentally determined activation volumes  $\Delta V_i$  of Mg, Fe and Mn reported by Chakraborty and Ganguly (1992) which account for the pressure effect on  $D_i$  in Eq. 3 at  $f_{\text{O}_2}$  defined by graphite– $\text{O}_2$  buffer. The activation volume of Ca ( $\Delta V_{\text{Ca}}$ ) was suggested to be equal to  $\Delta V_{\text{Mn}}$  since the ionic radius of Ca (1.12 Å) is closer to Mn (0.93 Å) than all the other divalent cations with available  $\Delta V$  (Ganguly et al. 1998).

The normalized diffusion coefficients of the major divalent cations are depicted in Fig. 12 (see Fig. 1 for compositional ranges). For the Alm–Prp diffusion couple, our data on  $D_{\text{Mg}}$  agree well with the results of Ganguly et al (1998). We find that Mg diffuses with the same rate in Sps–Prp and Alm–Prp diffusion couples (Fig. 1), as also reported by Ganguly et al. (1998) for Alm–Sps and Alm–Prp diffusion couples. Extrapolation to lower temperatures of our  $D_{\text{Mg}}$  is in agreement with normalized  $D_{\text{Mg}}$  in pure pyrope (Cygan and Lasaga 1985; Chakraborty and Rubie 1996) thus supporting the conclusion of several workers (e.g. Chakraborty and Rubie 1996; Ganguly et al 1998) that there is no break in Arrhenius slope between 1,400 and 750°C for  $D_{\text{Mg}}$ . Based on this consideration we conclude that CIP method may provide reasonable values of self-diffusion coefficients.

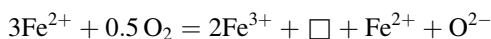
Available data on  $D_{\text{Fe}}$  are known only from the Alm–Sps and Alm–Prp diffusion couple experiments (Table 1). The slowest diffusion rate of  $\text{Fe}^{2+}$  in garnet was reported by Ganguly et al. (1998) for the Prp–Alm diffusion couple (Table 2). The difference of about  $\sim 1$  log unit for  $D_{\text{Fe}}$  from the Sps–Alm diffusion couple studied by Chakraborty and Ganguly (1992) was attributed to the enhancing effect of the Mn/Mg ratio in garnet on  $D_{\text{Fe}}$ . The magnitude of the effect seems to be variable: we found that the diffusion rate of Fe in the Alm–Prp diffusion couple is almost the same as reported for the Sps–Alm couple (Elphick et al. 1985; Loomis et al. 1985; Chakraborty and Ganguly 1992), whereas Gerasimov (1987) reported even higher values of  $D_{\text{Fe}}$  in the Alm–Prp diffusion couple (Fig. 12).

The diffusion rate of Ca remains the most controversial (Fig. 12). The lowest  $D_{\text{Ca}}$  is attributed to  $^{44}\text{Ca}$  self diffusion in grossular in the temperature range of 800–1,000°C at 1 atm and QFM buffer (Schwandt et al. 1996). The relatively low activation energy obtained in this study was recently supported (but with higher frequency factor) by Vielzeuf et al. (2007) for Ca–(Fe, Mg) interdiffusion at seeds/overgrowth interface which is lacking a physically distinctive boundary.  $D_{\text{Ca}}$  in our study is of 1–2 orders of magnitude higher than the interdiffusion coefficient of Vielzeuf et al. (2007). Both the datasets converge, however, at lower temperatures ( $T \sim 800^\circ\text{C}$ ) because of the different activation energies. Our fit on  $D_{\text{Ca}}$  is in a good

**Fig. 12** Arrhenius plot comparing data of this study (*solid heavy lines*) with earlier experimentally determined self-diffusion (and interdiffusion, see Table 1) coefficients of other workers normalized to a pressure of 1 GPa. **a** Fe, **b** Mn, **c** Mg, **d** Ca. Abbreviations related to diffusion couple (*solid lines, circles*) and tracer isotope coating experiments (*dashed lines*): CG92 Chakraborty and Ganguly (1992), CL85 Cygan and Lasaga (1985), CR96 Chakraborty and Rubie (1996), E85 Elphick et al. (1985), FE99 Freer and Edwards (1999), G89 Gerasimov (1987), G98 Ganguly et al. (1998), L85 Loomis et al. (1985), S95 Schwandt et al. (1995), S96 Schwandt et al. (1996), V07 Vielzeuf et al. (2007)



agreement with the data set of Carlson (2006) and individual values of  $D_{Ca}$  obtained by Ganguly et al. (1998) (Fig. 12d). The highest values of  $D$  for divalent cations were obtained by Freer and Edwards (1999): their Ca–(Fe, Mg) interdiffusion coefficient obtained under iron–wuestite buffer conditions is of several orders of magnitude higher than the  $D_{Ca}$  obtained in the present study. Normalization of their data to the conditions of graphite–oxygen buffer decreases the  $D$  by  $\sim 0.5$  log units owing to the last term in Eq. 3, i.e. the M1 vacancy ( $\square$ ) concentration in garnet which is controlled by the following redox reaction



cannot account for very high  $D_{Ca-(Fe, Mg)}$  suggested by Freer and Edwards (1999). The particular composition of grossular used in their experiments may have a critical effect on diffusion rate (see above).

The origin of these discrepancies in the diffusion data is not always clear. Even the self diffusion of the most studied element Mg there is a lack of consensus. For example, Chakraborty and Rubie (1996) pointed out that

the difference between their results and those by Schwandt et al. (1996) may be partly due to a compositional dependence of  $D_{Mg}$  in pyrope-rich garnets. However, Ganguly et al. (1998) argued that the compositional dependence couldn't reconcile these two data sets because Schwandt et al. (1995) used garnet of similar composition to that used by Cygan and Lasaga (1985). The latter dataset can be reconciled with the data of Chakraborty and Rubie (1996) when corrected for  $f_{O_2}$ . Schwandt et al. (1995) pointed out that differences in experimental techniques may be an important source of discrepancies. However, Chakraborty and Rubie (1996, p. 412) described a study by R. Cygan (unpublished data), who repeated three runs of Chakraborty and Rubie (1996) using their Tanzanian garnets and following the method of Schwandt et al. (1995). It was found that there is "reasonable agreement between data obtained using two completely different techniques employing different isotopes ( $^{26}\text{Mg}$  vs.  $^{25}\text{Mg}$ )". Thus difference in experimental techniques as well as garnet compositions may not be responsible for discrepancy of the results.

Cygan and Lasaga (1985) examined the crystal structure of the isotropic garnet in order to analyze the possible mechanism by which diffusion of Mg (and thus any other divalent cation which occupies triangular dodecahedral site) can occur. They emphasized that cation interstitials wouldn't be energetically favored due to the dense sublattice of the oxygens and suggested that for diffusion to occur it is necessary for the crystal lattice to possess significant number of Schottky type defects (vacancies). Since the diffusion mechanism doesn't change (at least for  $\text{Mg}^{2+}$ ) in the temperature range of 750–1,450°C, elastic strain energies may be of particular importance to explain discrepancies in the data. Van Orman et al. (2001) studied diffusion rates of five REE in diopside and found significant decrease of diffusion rates with increasing of ionic radius, which is in agreement with an elastic strain model. The same tendency has been found in the other minerals like zircon (Cherniak et al. 1997), plagioclase (Giletti and Shanahan 1997; La Tourrette and Wasserburg 1998) and periclase (Wuensch 1982), but not in garnet. Van Orman et al. (2002) demonstrated that there is no significant influence of ionic radius of Yb, Dy, Sm and Ce on diffusion rate in pyrope. Although lack of such an influence was explained by dissipation of the elastic strain energy, it was noted, that the reasons for such exceptional behavior of cations in garnets remains unclear (van Orman et al. 2002). This conclusion was recently reinforced by Tirone et al (2005) who studied self-diffusion coefficients of Gd, Nd, and Yb in pyrope and Sm and Nd in almandine.

The limited experimental data set on low-temperature experiments has been recently extended by Carlson (2006), who retrieved diffusion coefficients by modeling the evolution of diffusion profiles preserved in partially resorbed natural garnets from polymetamorphic terrains with well known thermal histories. Sets of data from two occurrences—the Llanos Uplift of central Texas and the contact aureole of the Makhacinekh Lake Pluton of northern Labrador—were treated by Carlson (2006) numerically in order to obtain the diffusion rates of the major divalent cations. It was found that there is a clear correlation between the frequency factor  $D^0$  and the unit cell dimension of the host garnet. This correlation was incorporated into a new model for calculating the diffusion rates of major divalent cations a wide range of garnet compositions (Carlson 2006). It is interesting to note that most of the measured self-diffusion coefficients of the present paper agree well with the predictions of Carlson's (2006) model at the same  $P$ ,  $T$ ,  $f_{\text{O}_2}$  and garnet composition (W. Carlson, personal communication): 30 of 38 values in Table 5 fall in the range of  $\pm 0.8 \log_{10}$  units, the approximate 95% confidence interval for all data in the model, which includes the compiled experimental data set of Carlson (2006), plus Carlson's data from natural crystals. The model predicts

strong enhancement of diffusion rates in Ca- and Mn-rich crystals: it makes possible to reconcile very fast diffusion rate of Ca suggested by Freer and Edwards (1999) with the data of this work and those by Ganguly et al (1998). The model of Carlson assumes that the activation energies of the principal divalent cations are similar, and thus the results of Schwandt et al. (1996) (DC method) and Vielzeuf et al. (2007) (SOI method) involving relatively low activation energies can't be directly attributed to the model.

#### Effect of inclusions

In modeling diffusion profiles in natural samples it is not always possible to avoid inclusion-rich garnets, and thus the diffusion data retrieved from gem-quality garnets are then applied to natural garnets with abundant mineral inclusions (e.g. Perchuk and Philippot 1997; Dachs and Proyer 2002; Faryad and Chakraborty 2005). Mineral inclusions in natural garnets may either remain inert and unreacted, or they may re-equilibrate with the host via chemical processes such as exchange/continuous reactions, or they may undergo polymorphic phase transformations. Chemical reactions normally affect garnet host compositions and thus are usually quite visible (e.g. Spear and Parrish 1996; Perchuk et al. 2005). Polymorphic phase transformations of inclusions usually lead to a system of radial (or concentric) cracks in garnet which reflect the existence of inclusion-related stress associated with dislocations and lattice distortion of the host garnet. Similar effects (but on a smaller scale) may occur around unreacted inclusions due to different elastic parameters as compared to the host garnet.

The common assumption in petrology that the diffusivities of the major cations are independent of the degree of impurity of the host garnet was justified by the lack of data. The present study provides a first comparative, albeit indirect evaluation of this assumption. We find that the diffusion rates of Mg and Fe in inclusion-rich garnets are systematically lower than within gem-quality crystals (Table 5, Figs. 11, 12). Nevertheless, we realize that the differences in the diffusion rates are within the substantial errors of the method on the one hand, and on the other hand require assessment of various parameters such as abundance, type and distribution of mineral inclusions, number of defects within the crystalline structure of garnet, distance from inclusion(s) and the particular composition of the garnet involved.

#### Advantages and pitfalls of the CIP crystals-in-powder method

Most of the data on the diffusivity of divalent cations in garnet obtained so far are based on the SC method (see

Table 1). Considering the lack of general agreement on the diffusion coefficients of some of the principal divalent cations (e.g. Ca and Fe) in garnet (Fig. 12), we believe that the alternative experimental techniques outlined in the introduction need to be considered as well. The general advantages of the method used in our study are (1) the relatively straightforward preparation of starting materials and loading of capsules, (2) the opportunity to study several diffusion couples simultaneously, and (3) the robust preservation of the diffusion-couple interface. On the basis of this last point, most runs in our study have been successful. There are, however, some inherent challenges in different stages of our study. One is that the spherical and/or idiomorphic grains may have shifted from their original position during pressurizing of the capsule. Thus it may be difficult to ensure sectioning of the crystals close to their grain centers after the run. Nevertheless, this problem arises only when there are several grains of a size much smaller than the inner diameter of the capsule. The problem can be resolved by using only spherical grains of a diameter close to the inner diameter of the capsule. Any longitudinal axial section of the post-run capsule (e.g. run DM5) will a priori be closely located to the centre of the crystals. Furthermore, successive grinding of single crystals can also lead to optimum sections. In this case, however, the goal of a simultaneous study of several diffusion couples is sacrificed.

The advantage of multi-couple diffusion experiments brings with it uncertainties related to the size of the capsules. Firstly, in spite of their high thermal conductivity, Pd capsules cannot smooth out completely the thermal gradient within the capsule, and, as follows from the numerical modeling (see above), the thermocouple shows only a minimum run temperature. The maximum deviation from the thermocouple reading occurs close to the center of the capsule. This yields maximum uncertainties of  $D$  and thus leads to an overestimation of  $D$  on a scale indicated in Fig. 11a. However, in spite of these uncertainties, we obtained  $D$  values which are close to most published datasets (Fig. 12). Second, pressurization of the cell in piston-cylinder experiments may lead to distortion of the graphite furnace and to diking of the glass into fractures in the furnace. This may cause local hot spots in the furnace. Experiments with relatively long capsules and single thermocouples may be vulnerable to this problem if it happens to occur. However, as noted above, careful inspection of the furnaces after the runs revealed no distortion of the heaters near the capsules. This was confirmed by lack of the extra long diffusion profiles. To further develop the method, the design of the pressure cell can be improved by using (a) a tantalum or molybdenum ring between the graphite capsule and the graphite furnace as suggested earlier (Elphick et al. 1985; Chakraborty and

Ganguly 1991) to minimize furnace distortion and the temperature gradient over the capsule, and (b) by decreasing the capsule length and introducing fewer spherical samples in the powdered matrix.

One of the major problems of diffusion experiments with single crystals in sintered powder is the potential effect of channeling of cations along grain boundaries. To better understand why channeling of cations along grain boundaries can be significant in some domains (e.g. Fig. 6 in this study and Elphick et al. 1985, p. 37) and absent in others (e.g. Fig. 5a), we performed numerical experiments using FEMLAB<sup>®</sup> software (see below). FEMLAB allows the 2D modeling of various diffusion problems, including simultaneous grain-boundary and volume diffusion fluxes such as those to be expected in our runs. These results are presented in the next section.

#### Grain-boundary diffusion within the interdiffusion zone: numerical modeling and experimental observations

Electron microprobe profiles normal to the interface of a diffusion couple occasionally reveal different types of irregularities. The affected domains may contain plateau-like segments, “shoulders” and flexures (Fig. 13). These irregularities most often occur on the pyrope (sintered) side of profiles, but have also rarely been observed on the spessartine and almandine sides. Irregular domains with both gentle and steep slopes of the concentration gradients were originally documented as “shoulders” in SC runs with sandwiched crystals (Elphick et al. 1985; Ganguly et al. 1998). Elphick et al. (1985) suggested that fractures parallel to the interface “extended” the profile (their Fig. 5). Ganguly et al. (1988) introduced “shoulders” within interdiffusion zones of almandine crystals and characterized them as a “not well understood” phenomenon (their Fig. 1a). The following results of 2D diffusion modeling provide new insights on the origin of these different types of irregularities in diffusion profiles.

The 2D diffusion calculations were solved in the FEMLAB<sup>®</sup> (Comsol, Inc.) environment. Transient analysis mode has been applied to retrieve interdiffusion profiles generated by an experimental diffusion couple consisting of single-crystal garnet and sintered matrix of garnet of dissimilar compositions. A finite area  $18 \times 18 \mu\text{m}$  in size was considered. It consisted of two rectangular domains (Figs. 14, 15) with “insulation/symmetry” boundary condition ( $-D\nabla c = 0$ ) for the exterior margins and “continuity” ( $-D\nabla c$ ) for the mutual contact. The size was chosen large enough to allow volume diffusion penetration. One of the domains was chosen to simulate Alm<sup>a</sup> garnet (Table 3) characterized by a normalized concentration of Mg ( $N_{\text{Mg}} = X_{\text{Prp}}/(X_{\text{Prp}} + X_{\text{Alm}})$ ). The other domain

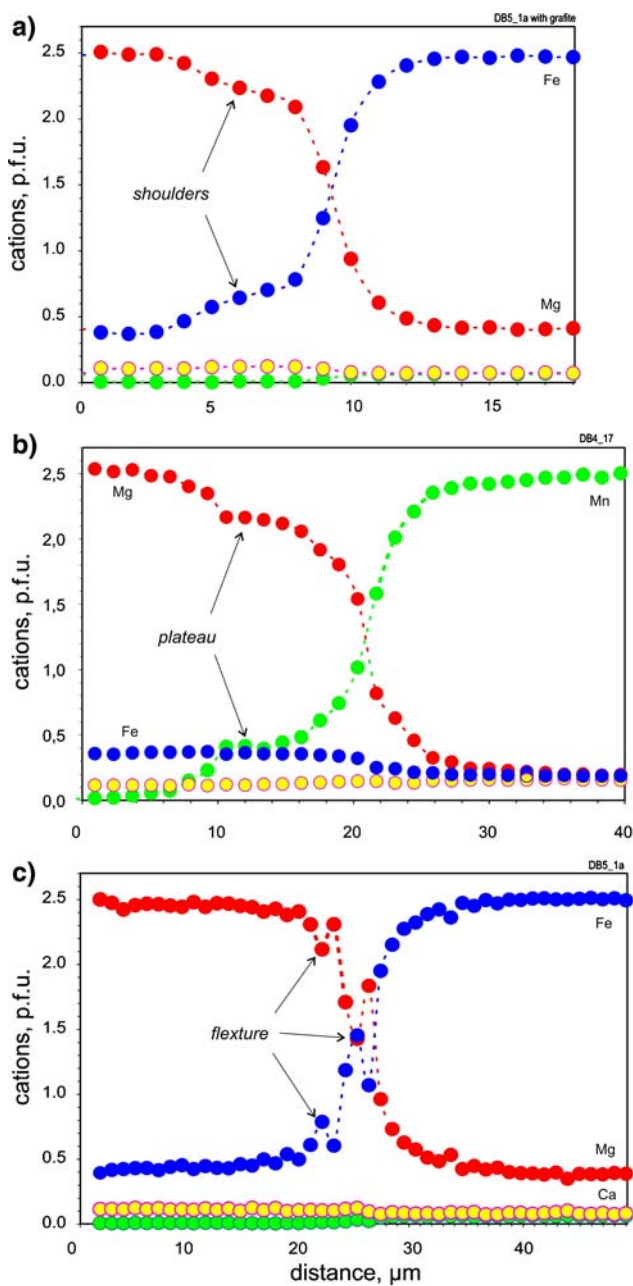


**Fig. 13** Irregularities in interdiffusion profiles caused by grain-boundary diffusion: **a** “shoulders” on the pyrope side of the type 1 Alm–Prp diffusion couple of run DB5 (with graphite); **b** plateau-like segment on the pyrope side of the Sps–Prp diffusion couple of run DB4; **c** flexures within the type 1 Alm–Prp diffusion couple of run DB5

represents the sintered matrix of pyrope composition (Table 3). As a first step we tested the program by modeling pure Fe–Mg interdiffusion between almandine (Alm<sup>a</sup>) and pyrope garnets at the *P–T–t* conditions of run DB1 (see Table 5 for the conditions and self-diffusion coefficients). Because the simulated profile was in good agreement with the experimental data points as well as with the fit provided

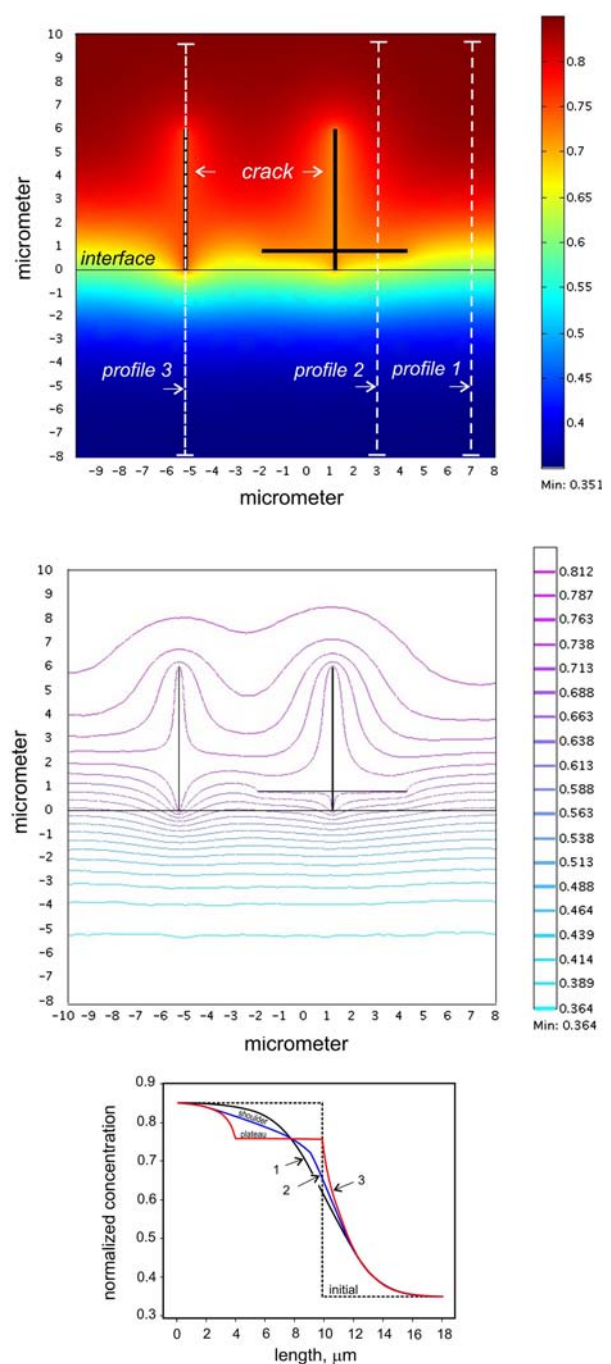


**Fig. 14** “Shoulders” and plateau-like segments as irregularities of the interdiffusion profiles. Results of numerical modeling (FEMLAB software) under conditions of run DB1 (1,300°C, 2.6 GPa, 96 h). Volume self-diffusion coefficients  $D^V = D_{Mg} = D_{Fe} = 10^{-17} \text{ m}^2/\text{s}$  (close to those in the run DB1, Table 5), grain-boundary diffusion coefficient  $D^{GB}$  within the cracks of width 1 nm was assumed according to the ratio  $\log(D^{GB}/D^V) = 4$ . **a** Design of the modeled area of size  $18 \times 18 \mu\text{m}$ . The interface and fractures within pyrope are shown as heavy lines. *Dashed lines* position of profiles. **b** Fitted distribution of normalized concentration of Mg ( $Mg/(Mg + Fe)$ ). **c** Normalized concentration profiles along the profiles depicted in **a**. Note that grain-boundary diffusion may increase compositional gradient. See text for further details

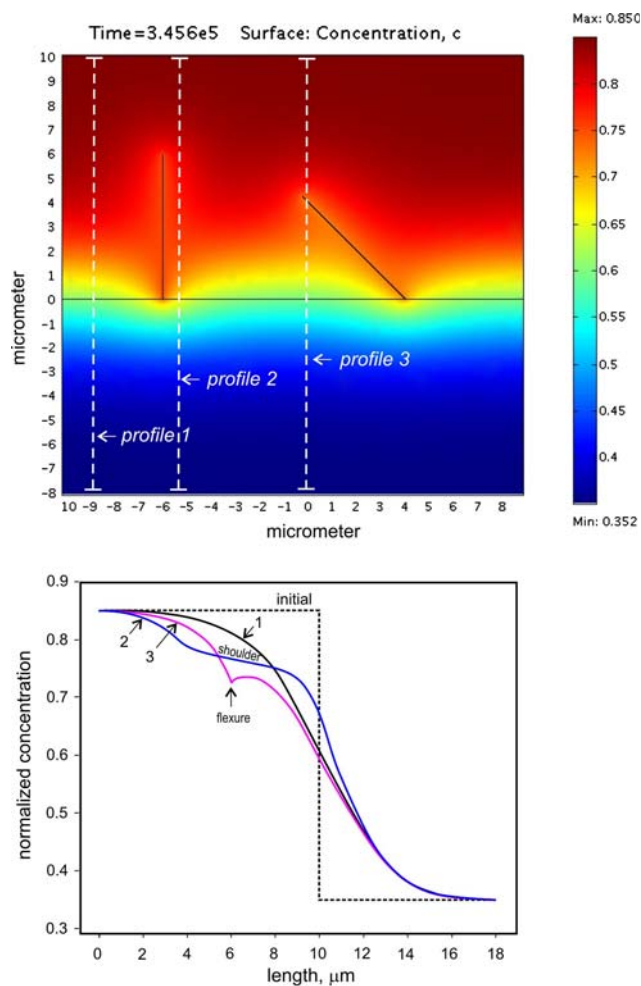


**Fig. 15** “Shoulders” and flexures within interdiffusion profiles. Results of numerical modeling (FEMLAB software). Conditions of the numerical experiment are the same as in Fig. 14. **a** Design of the modeled area of size  $19 \times 28 \mu\text{m}$ . The interface and fractures within pyrope are shown as heavy lines. *Dashed lines* position of the profiles. **b** Normalized concentration profiles along the profiles depicted in **a**

by the DXL program, we turned to the more complicated task. Accordingly, cracks were inserted in the pyrope domain to approximate the diffusion in certain areas in a sintered pyrope where volume diffusion is concomitant with flux along grain boundaries. Different positions and orientations were considered to check their relative contribution to the compositional profiles. We regarded the cracks as slabs of 1 nm wide, i.e. like the width of grain boundaries (Joesten 1991; Farver et al. 1994). Zero concentration was assumed for the slab as initial condition. Modeling reveals that the contribution of the initial concentration of the crack to the final profile is negligible. The profile mainly depends on the concentration of the host garnet. The boundary condition of “continuity” was applied for the slab margins. The diffusivity of cations in the slabs (grain-boundary diffusion coefficient,  $D^{\text{GB}}$ ) is

unknown for garnet. We present here the results obtained with the ratio  $\log(D^{\text{GB}}/D^{\text{V}}) = 4$  as established for some oxides and silicates (Joesten 1991). For simplicity, a volume diffusion  $D^{\text{V}} = 10^{-17} \text{ m}^2/\text{s}$  was assumed for the diffusivity of both Fe and Mg in garnet (close to the  $D_{\text{Fe}}$  and  $D_{\text{Mg}}$  retrieved from run DB1, Table 5). The mesh was initialized by the program and then refined at the contact of the two domains and in the crack-related areas.

For example, plateau-like segments were found in the profiles related to the cracks (grain boundaries) oriented normal to the interface, i.e. parallel to the volume diffusion flux (Fig. 14, profile 3; compare with Fig. 13b). Profiles situated close to such cracks, or those that have a significant crack-related flux component contain “shoulders” (Fig. 14, profile 2, Fig. 15 profile 2; compare with Fig. 13a) similar to those observed by Ganguly et al. (1998, their Fig. 1a) in the SC diffusion-couple runs. Thus “shoulders” represent volume diffusion of cations related to grain-boundary diffusion. Cracks that do not follow the direction of volume diffusion flux do not enhance diffusion penetration away from the interface. The corresponding leakage of components along the crack is responsible for the flexures in profiles (Fig. 15, profile 3; compare with Fig. 13c). Note that strong volume diffusion near the interface may attenuate flexures related to the crack (Fig. 14, profile 2).

In general, the effect of the cracks on the interdiffusion profile increases if they are located closer to the interface and oriented normal to it. Interestingly, the flux along such grain boundaries strongly modifies the shape of the profile on the both sides of the interface (Fig. 14). The more the crack is inclined from a normal line to the interface, the less it contributes to the interdiffusion profile. Cracks located parallel to the interface fail to affect the interdiffusion profile only when they are isolated. The same crack may, however, modify the profile if connected with another crack that effectively transports components.

The enhanced migration of components along the grain boundaries of the matrix or along the microcracks in the crystals deserves further investigation, because this feature is also a clue for deciphering the rates of grain-boundary diffusion in garnet.

## Concluding remarks

This paper presents a novel format for studying cation diffusivity in garnet. We demonstrate for the first time the possibility of studying several diffusion couples in a single run. Thus the duration of experimental study and the risk of failure of expensive experimental equipment (e.g. tungsten carbide cores) was decreased considerably. Another advantage of this type of procedure is that the diffusion

profiles were induced in the same capsule in a single run, i.e. under almost similar  $P$ – $T$ – $t$ – $f_{\text{O}_2}$  conditions, allowing direct comparison of the diffusion rates in different diffusion couples. Although further optimization of the experimental procedure is possible, we believe that the method outlined in this paper deserves further applications in studies of rates of volume and/or grain-boundary diffusion in minerals.

**Acknowledgments** We thank D. Vielzeuf for fruitful discussions and critical reading of the first draft of the manuscript, S. Chakraborty for discussions, R. Neuser for assistance during SEM work and T. Westphal for preparation of the samples. A.L.P. was supported by an Alexander von Humboldt Foundation Research Fellowship, RFBR grant N 06-05-65204, and by the Centre National Recherche Scientifique (Devison Alpes), France. Constructive comments of J. Ganguly, J. Van Orman, W. Carlson and an anonymous reviewer of different versions of the manuscript are highly appreciated. T. Grove is thanked for helpful editorial comments.

## References

- Béjina F, Jaoul O, Liebermann RC (2003) Diffusion at high pressure: a review. *Phys Earth Planet Int* 139:3–20
- Carlson WD (2006) Rates of Fe, Mg, Mn, and Ca diffusion in garnet. *Am Mineral* 91:1–11
- Carlson WD, Schwarze E (1997) Petrological significance of prograde homogenization of growth zoning in garnet: an example from the Llano Uplift. *J Metam Geol* 15:631–644
- Chakraborty S, Ganguly J (1991) Compositional zoning and cation diffusion in garnets. *Adv Phys Geochem* 8:121–175
- Chakraborty S, Ganguly J (1992) Cation diffusion in aluminosilicate garnets: experimental determination in spessartine-almandine diffusion couples, evaluation of effective binary diffusion coefficients, and applications. *Contrib Mineral Petrol* 111:74–86
- Chakraborty S, Rubie DC (1996) Mg tracer diffusion in aluminosilicate garnets at 750–850°C, 1 atm. and 1300°C, 8.5 GPa. *Contrib Mineral Petrol* 122:406–414
- Cherniak DJ, Hanchar JM, Watson EB (1997) Rare-earth diffusion in zircon. *Chem Geol* 134:289–301
- Crank J (1975) *The mathematics of diffusion*. Oxford University Press, Oxford
- Cygan RT, Lasaga AC (1985) Self-diffusion of magnesium in garnet at 750°C to 900°C. *Am J Sci* 285:328–350
- Dachs E, Proyer A (2002) Constraints on the duration of high-pressure metamorphism in the Tauern Window from diffusion modelling of discontinuous growth zones in eclogite garnet. *J Metam Geol* 20:769–780
- Elphick SC, Ganguly J, Loomis TP (1985) Experimental determination of cation diffusivities in aluminosilicate garnets I. Experimental methods and interdiffusion data. *Contrib Mineral Petrol* 90:36–44
- Farver JR, Yund RA, Rubie DC (1994) Magnesium grain boundary diffusion in forsterite aggregates at 1000–1300°C and 0.1 MPa to 10 GPa. *J Geophys Res* 99:19809–19819
- Faryad SW, Chakraborty S (2005) Duration of Eo-Alpine metamorphic events obtained from multicomponent diffusion modeling of garnet: a case study from the Eastern Alps. *Contrib Mineral Petrol* 150:306–318
- Fockenberg T (1998) An experimental investigation on the  $P$ – $T$  stability of Mg-staurolite in the system MgO–Al<sub>2</sub>O<sub>3</sub>–SiO<sub>2</sub>–H<sub>2</sub>O. *Contrib Mineral Petrol* 130:187–198
- Freer R (1979) Experimental measurement of cation diffusion in almandine garnet. *Nature* 280:220–222
- Freer R (1987) A discussion of “Experimental determination of cation diffusivities in aluminosilicate garnets. I. Experimental methods and interdiffusion data” by SC Elphick, J Ganguly and TP Loomis. *Contrib Mineral Petrol* 97:535–536
- Freer R, Edwards A (1999) An experimental study of Ca–(Fe, Mg) interdiffusion in silicate garnets. *Contrib Mineral Petrol* 134:370–379
- Ganguly J, Loomis TP, Elphick SC (1987) Experimental determination of cation diffusivities in aluminosilicate garnets: reply to the discussion by Freer of Part I, and correction of Mn tracer diffusion data in Part II. *Contrib Mineral Petrol* 97:537–538
- Ganguly J, Bhattacharya RN, Chakraborty S (1988) Convolution effect in the determination of compositional profiles and diffusion coefficients by microprobe step scans. *Am Mineral* 73:901–909
- Ganguly J, Chakraborty S, Sharp TG, Rumble D (1996) Constraint on the time scale of biotite-grade metamorphism during Acadian orogeny from a natural garnet–garnet diffusion couple. *Am Mineral* 81:1208–1216
- Ganguly J, Cheng W, Chakraborty S (1998) Cation diffusion in aluminosilicate garnets: experimental determination in pyrope–almandine diffusion couples. *Contrib Mineral Petrol* 131:171–180
- Ganguly J, Dasgupta S, Cheng W, Neogi S (2000) Exhumation history of a section of the Sikkim Himalayas, India: records in the metamorphic mineral equilibria and compositional zoning of garnet. *Earth Planet Sci Lett* 183:471–486
- Gerasimov VY (1987) Experimental study on Mg–Fe interdiffusion in garnets. *Trans USSR Acad Sci* 295:684–688
- Gerasimov VY, Savko KA (1995) Geospeedometry and thermal evolution of garnet–cordierite metapelites of Voronezh crystallize massif. *Petrology* 6:563–577
- Giletti BJ, Shanahan TM (1997) Alkali diffusion in plagioclase feldspar. *Chem Geol* 139:3–20
- Hernlund J, Leinenweber K, Locke D, Tyburczy JA (2006) A numerical model for steady-state temperature distributions in solid-medium high-pressure cell assemblies. *Am Mineral* 91:295–304
- Jaoul O, Sautter V (1999) A new approach to geospeedometry based on the compensation law. *Phys Earth Planet Inter* 110:95–114
- Jiang J, Lasaga AC (1990) The effect of post-growth thermal events on the growth-zoned garnet: implications for metamorphic  $P$ – $T$  history calculations. *Contrib Mineral Petrol* 105:454–459
- Joesten R (1991) Grain-boundary diffusion kinetics in silicate and oxide minerals. *Adv Phys Geochem* 8:345–395
- Konrad-Schmolke M, Handy MR, Babist J, O’Brien PJ (2005) Thermodynamic modelling of diffusion-controlled garnet growth. *Contrib Mineral Petrol* 149:181–195
- La Tourrette T, Wasserburg GJ (1998) Mg diffusion in anorthite: implications for the formation of early solar system planetesimals. *Earth Planet Sci Lett* 158:91–108
- Lasaga AC (1979) Multicomponent exchange and diffusion in silicates. *Geochim Cosmochim Acta* 3:455–469
- Lasaga AC (1983) Geospeedometry: an extension of geothermometry. *Adv Phys Geochem* 3:81–114
- Loomis TP, Ganguly J, Elphick SC (1985) Experimental determination of cation diffusivities in aluminosilicate garnets II. Multicomponent simulation and tracer diffusion coefficients. *Contrib Mineral Petrol* 90:45–51
- Medaris LG, Wang HF, Misar Z, Jelinek E (1990) Thermobarometry, diffusion modelling and cooling rates of crustal garnet peridotites: two examples from the Moldanubian zone of the Bohemian massif. *Lithos* 25:189–202

- Muncill GE, Chamberlain CP (1988) Crustal cooling rates inferred from homogenization of metamorphic garnets. *Earth Planet Sci Lett* 87:390–396
- O'Brien PJ, Vrana S (1995) Eclogites with short-lived granulite facies overprint in the Moldanubian Zone, Czech Republic: petrology, geochemistry and diffusion modeling of garnet zoning. *Geol Rudsch* 84:473–488
- Olker B, Altherr R, Paquin J (2003) Fast exhumation of the ultrahigh-pressure Alpe Arami garnet peridotite (Central Alps, Switzerland): constraints from geospeedometry and thermal modeling. *J Metam Geol* 21:395–402
- Osager L (1945) Theories and problems of liquid diffusion. *Ann N Y Acad Sci* 46:241–265
- Patiño Douce AE, Harris N (1998) Experimental constraints on Himalayan anatexis. *J Petrol* 39:689–710
- Perchuk AL, Philippot P (1997) Rapid cooling and exhumation of eclogitic rocks from the Great Caucasus, Russia. *J Metam Geol* 15:299–310
- Perchuk AL, Philippot P (2000) Geospeedometry and timescales of high-pressure metamorphism. *Intern Geol Rev* 42:207–223
- Perchuk AL, Gerya TV (2005) Burial and exhumation dynamics of eclogites in the Yukon–Tanana Terrane, Canadian Cordillera: petrological reconstructions and geodynamic modeling. *Petrology* 13:253–266
- Perchuk AL, Philippot P, Erdmer P, Fialin M (1999) Rates of thermal equilibration at the onset of subduction deduced from diffusion modeling of eclogitic garnets, Yukon–Tanana terrain. *Geology* 27:531–534
- Perchuk AL, Burchard M, Maresch WV, Schertl H-P (2005) Fluid-mediated modification of garnet interiors under ultrahigh-pressure conditions. *Terra Nova* 17:545–553
- Pickering JM, Schab BE, Johnston AD (1998) Off-center hot spots: double thermocouple determination of the thermal gradient in a 1.27 cm (1/2 in.) CaF<sub>2</sub> piston-cylinder furnace assembly. *Am Mineral* 83:228–235
- Schertl H-P, Schreyer W, Chopin C (1991) The pyrope–coesite rocks and their country rocks at Parigi, Dora Maira massif, Western Alps: detailed petrography, mineralogy and P-T-path. *Contrib Mineral Petrol* 108:1–21
- Schilling F, Wuender B (2004) Temperature distribution in piston-cylinder assemblies: numerical simulations and laboratory experiments. *Eur J Mineral* 16:7–14
- Schwandt CS, Cygan RT, Westrich HR (1995) Mg self-diffusion in pyrope garnet. *Am Mineral* 80:483–490
- Schwandt CS, Cygan RT, Westrich HR (1996) Ca self-diffusion in grossular garnet. *Am Mineral* 81:448–451
- Spear FS, Parrish R (1996) Petrology and petrologic cooling rates of the Valhalla Complex, British Columbia, Canada. *J Petrol* 37:733–765
- Takahashi E (1986) Melting of the dry peridotite KLB-1 up to 14 Gpa: implications of the origin of peridotitic upper mantle. *J Geophys Res* 91/B8:9367–9382
- Tirone M, Ganguly J, Dohmen R, Langenhorst F, Hervig R, Becker H-W (2005) Rare earth diffusion kinetics in garnet: experimental studies and applications. *Geochim Cosmochim Acta* 69:2385–2398
- Toor HL (1964) Solution of the linearized equations of multicomponent mass transfer: II. Matrix methods. *J Am Inst Chem Eng* 8:460–465
- Tracy RJ (1982) Compositional zoning and inclusions in metamorphic minerals. *Rev Mineral MSA* 10:355–397
- Trepmann CA, Stoeckert B, Chakraborty S (2004) Oligocene trondhjemitic dikes in the Austroalpine basement of the Pfunderer Berge, Südtirol: level of emplacement and metamorphic overprint. *Eur J Mineral* 16:641–659
- Van Orman JA, Grove TL, Shimizu N (2001) Rare earth element diffusion in diopside: influence of temperature, pressure, and ionic radius, and an elastic model for diffusion in silicates. *Contrib Mineral Petrol* 141:687–703
- Van Orman JA, Grove TL, Shimizu N, Layne GD (2002) Rare earth element diffusion in a natural pyrope single crystal at 2.8 GPa. *Contrib Mineral Petrol* 142:417–424
- Vielzeuf D, Lupulescu A, Perchuk AL, Laporte D, Baronnet A, Addad A (2005a) Uphill diffusion and zero flux planes in garnets: an experimental and ATEM study. *TMS Lett* 2:89–90
- Vielzeuf D, Veschambre M, Brunet F (2005b) Oxygen isotope heterogeneities and diffusion profile in composite metamorphic–magmatic garnets from the Pyrenees. *Am Mineral* 90:463–472
- Vielzeuf D, Baronnet A, Perchuk AL, Laporte D, Baker M (2007) Calcium diffusivity in aluminosilicate garnets: an experimental and ATEM Study. *Contrib Mineral Petrol* 154:153–170
- Vignaroli G, Rossetti F, Bouybaouene M, Massonne H-J, Theye T, Faccenna G, Funicello R (2005) A counter-clockwise P-T path for the Voltri Massif eclogites (Ligurian Alps, Italy). *J Metam Geol* 23:533–555
- Watson EB, Wark DA, Price JD, Van Orman JA (2002) Mapping the thermal structure of solid-media pressure assemblies. *Contrib Mineral Petrol* 142:640–652
- Willner AP, Glodny J, Gerya TV, Godoy E, Massonne H-J (2004) A counterclockwise P–T–t path of high-pressure/low-temperature rocks from the Coastal Cordillera accretionary complex of south-central Chile: constraints for the earliest stage of subduction mass flow. *Lithos* 75:283–310
- Wuensch BJ (1982) Diffusion in stoichiometric close-packed oxides. In: Beniere F, Catlow CRA (eds) *Mass transport in oxides*. NATO-ASI, New York, pp 353–376